TOWARDS A NEW GENERATION OF NONVOLATILE MEMORY DEVICES: CREATION

AND MANIPULATION OF TOPOLOGICAL MAGNETIC STRUCTURES BY ELECTRIC

CURRENT

A Thesis

by

DAVI ROHE SALOMON DA ROSA RODRIGUES

Submitted to the Office of Graduate and Professional Studies of
Texas A&M University
in partial fulfillment of the requirements for the degree of

DOCTOR OF PHILOSOPHY

Chair of Committee,	Artem Abanov
Committee Members,	Valery Pokrovsky
	Wenhao Wu
	Andrew Comech
Head of Department,	Grigory Rogachev

August 2018

Major Subject: Physics

ABSTRACT

In this thesis we propose a novel method to study the dynamics of topological magnetic textures. Based on the stability of these objects, scaling and symmetry arguments, we show that, despite the complexity of the micromagnetic model, the electric and magnetic driven dynamics can be described in terms of a few relevant dynamical parameters. This method reproduces well known behaviors reported in the literature without the assistance of sophisticated micromagnetic numerical calculations. Moreover, it allows for the study of new phenomena relevant for proposing new memory devices based on topological textures.

Based on a specific configuration of a nanowire with a strong pinning point, we predict a periodic injection of domain walls by all electrical means. Our analytical results reveal the existence of a critical current. For currents below the critical current, the magnetic configuration is stable and fully defined by a single parameter. For currents slightly above the critical current, this parameter becomes dynamical and is associated to the periodic injection of domain walls into the nanowire. The period is given by a universal exponent $T \sim (j - j_c)^{1/2}$. The process is very general and independent of microscopic details. A major feature is that the process is independent of "twisting" terms or applied external magnetic field.

We also propose a Hamiltonian dynamics formalism for the current and magnetic field driven dynamics of ferromagnetic and antiferromagnetic domain walls in one-dimensional systems. We obtain Hamiltonian equations for pairs of the dynamical parameters that describe the low energy excitations of domain walls. This model independent formalism includes both the undamped and damped dynamics. We use it to study current induced domain wall motion in ferromagnetic and antiferromagnetic materials. In the second material, we include also the influence of magnetic fields and predict an orientation switch mechanism for antiferromagnetic domain walls which can be tested experimentally.

Moreover, we extend the formalism from nanowires to thin-films and study extended domain walls as string objects. The description includes the dynamics of vortices and curvatures along

the domain wall as well as boundary effects. We provide an effective action that describes the dynamics of domain walls with periodic boundary conditions. By considering closed domain walls, we included the dynamics of smoothly deformed skyrmions in the large radius limit. Our theory provides an analytical description of the excitation modes of magnetic skyrmions in a natural way. The method developed along the thesis proves to be rich and powerful, being crucial for the development of a new generation of memory devices based on magnetic topological textures.

DEDICATION

To the benefit of all. May this project improve the life of all who struggle with slow computers

and their heating in the future.

ACKNOWLEDGMENTS

shorter than my gratitude. Last but not least, I would like to specially thank Josefina for being by my side in the final stressful moments.

CONTRIBUTORS AND FUNDING SOURCES

Contributors

This work was supported by a thesis committee consisting of Professor Artem AbanovĂŞ and Professors Valery Pokrovsy and Wenhao Wu of the Department of Physics and Astronomy and Professor Andrew Comech of the Department of Mathematics.

The analyses depicted in Chapter 3 were conducted in collaboration with Professor Jairo Sinova and Doctors Karin Everschor-Sitte, Matthias Sitte and Thierry Valet and it was published in 2016 in an article listed References. [1]. The analyses depicted in Chapter 4 were conducted in collaboration with Professors Jairo Sinova and Oleg Tretiakov and Doctor Karin Everschor-Sitte and it was published in 2017 in an article listed in References. [2] The analyses depicted in Chapter 5 were conducted in collaboration with Professor Jairo Sinova and Doctor Karin Everschor-Sitte and it was accepted for publication in 2018 in an article listed in the References. [3]

Funding Sources

NOMENCLATURE

LLG	Landau-Lifshitz-Gilbert
FM	Ferromagnetic
AFM	Antiferromagnetic
DW	Domain Wall
DMI	Dzyaloshinskii-Moryia interaction
SOT	Spin orbit torque
STT	Spin transfer torque

TABLE OF CONTENTS

LIST OF FIGURES

1. INTRODUCTION

1.1 Spintronics

In the past decades, the progress in the relatively young and application-driven field of spintronics has paved the way towards novel solutions for the demand of portable, high speed and high storage capacity devices. Spintronics was founded by the 2007 Nobel prize awarded work on giant magnetoresistance (GMR) and its goal is to exploit the spin degree of freedom in addition to the charge degree of freedom of an electron. [6] The current technological paradigm for computational devices is based only on the charge degree of freedom and currently faces obstacles towards its improvement. As society moves towards a more gadget-integrated life-style, in order to satisfy the increasing demand for smaller, faster and more efficient devices, new paradigms have been considered. In this thesis we will present current developments in spintronics and their applications to memory devices.

The current paradigm for computers are the use of transistor technology. It is based on semiconductor devices and the charge degree of freedom of the electron. This concept has driven the information-technology for more than sixty years and is currently facing obstacles towards its progress. [7] The technology invented in 1947 has inspired George Moore in 1965 to predict an exponential trend for the increase in the density of transistors in computer-devices. This trend was called *Moore's Law*. [8] In 2009, an analogous observation was done by Mark Kryder concerning the hard drive capacity, the projection was called *Kryder's Law*. The scalability of this technology was reliable for more than five decades. [9] The current limits faced by the state-of-the-art proposed devices, however, discourage further developments. Even though there are proposals for new ways to accommodate a higher density of components, the efficiency of each individual component hasn't increased significantly in the past few years. This imposes a fundamental obstacle given the limits on heat removal capacity. [10] The difficulties faced by the transistor technology have motivated the search for new technologies for computational devices.

A promising alternative candidate is the conjunct use of electrical and magnetic phenomena. The non-volatility of magnetization configurations has been exploited for applications in memory devices since the end of the nineteenth century. [11] In the past decades, the discovery of new methods to explore the interaction between the electric currents and the magnetic properties, given initially by the GMR effect, has given rise to a diverse range of applications. Moreover, the use of new nanoscale properties of magnetic configurations and their electric current and light driven dynamics has stimulated new and more efficient approaches. [12, 13, 6] The field that studies this new physics was called spintronics.

Some nanoscale objects of fundamental importance in spintronics are topological magnetic textures. They have attracted great interest in particular in the last decade due to their applications for memory and logic devices. [13] An evidence of this increasing interest is the recent increasing number of review papers on the subject. [14, 6, 15] The stability of these objects, even in the presence of external perturbations and temperature effects, is one of the main properties that supports them as reliable memory units. Another relevant property is the particle-like behavior under applied current and magnetic fields. These features have motivated an intense and diverse effort to obtain the means to create and manipulate topological magnetic objects. [16, 17, 18, 19, 20, 21, 22, 23] In this thesis, we will present theoretical results on creation of topological magnetic textures in nanowires and a description of current and field driven dynamics of topological textures in nanowires and thin-films.

1.2 Micromagnetism and topological textures

Micromagnetism is the dynamical theory of magnetic textures in the continuous approximation of a ferromagnetic or antiferromagnetic structure. [24] Ferromagnetic and antiferromagnetic materials can be modeled as a discrete lattice of magnetic moments interacting with each other, with an electronic field and with external perturbations. From the characteristic strengths of the interactions, it is possible to obtain natural scales for the dynamical behaviors. In the case where the natural length scale is much bigger than the lattice size, a continuous approximation for the discrete lattice is allowed, see Fig. 1.1. In this context, Landau and Lifshitz obtained in the 30's a

2

set of equations that describes the dynamics of the continuous magnetization configuration called *micromagnetic equations*. [25]
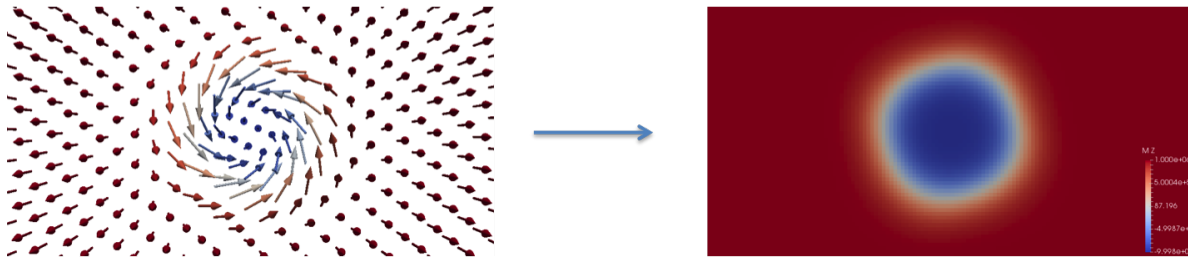
Figure 1.1: A representation of the micromagnetic modeling of the discrete lattice of magnetic moments. On the right pannel we see the continuous version of the discrete lattice of the left pannel. The colors represent the component of the magnetization normal to the plane, ranging from out-of-plane to in-plane orientations.

An interesting aspect of the description of magnetic textures as continuous vectorial fields is the emergency of topological properties. Topology is the area of Mathematics that studies properties that are preserved under smooth transformations. Topology has a broad range of application in physics, including in particle physics, cosmology and condensed matter physics. An evidence of the importance of these applications is the fact that a work based on this concept was awarded the 2016 Nobel prize in Physics. A field of topology with particular interest to condensed matter physics is the homotopy theory, which is crucial for the description of topological solitons. In the context of micromagnetism, topological solitons appear as topological magnetic textures.

In mathematical terms, topological solitons are classical solutions of the equations of motion that are homotopically different from the ground state. This means that it is impossible for these objects to dynamically decay into the vacuum state, and, therefore, are stable against fluctuations and external perturbations. The first example of these solutions applied to physics was proposed by Skyrme to explain the stability of elementary particles. [26] These solutions were called *skyrmions*. Later on, skyrmions received a very precise mathematical description and gained importance in other fields such as condensed matter physics. Another topological soliton of major importance

are *domain walls*. These solitons emerge in systems with spontaneously broken discrete symmetries. Skyrmions and domain walls can be observed as stable topological textures in magnetic samples. [13, 15, 24, 27, 28, 29, 30, 31, 32]

The stability of topological magnetic textures is of significant relevance for studying their dynamics. Even though the micromagnetic equations are highly complicated non-linear and non-local equations with an infinite degrees of freedom, the low energy excitation dynamics of these topological objects can be described by just a finite set of dynamical parameters. [33, 34, 35, 36] This grants them a particle-like behavior. From this point of view, it is possible to effectively describe systems of topological textures only in terms of the relevant dynamical parameters and disregarding microscopic details. [2]

A macroscopic and effective description of the dynamics in terms of a finite set of relevant dynamics parameters and minimal requirements is the guiding principle of the theoretical results presented in this thesis. By analyzing the underlying micromagnetic description of stable solutions, we have identified the relevant dynamical parameters that describes the small energy excitations. Moreover, by taking into account only these dynamical parameters, we obtained the minimal requirements for the creation of topological textures and their manipulation with external magnetic fields and electrical currents. The microscopic detail independent formalism proved to be robust and powerful. It reproduced well known facts and also allowed for the search of new dynamical behaviors.

1.3 Overview

This thesis is organized as follows: In the Methods Chapter 2.1, we introduce fundamental aspects of the micromagnetic model. We will explain the Landau-Lifshitz-Gilbert equation and the relevant effective interactions. The dynamical equation will be both derived from an action through a variational principle and from the Hamiltonian formalism. As relevant solutions of the dynamical equations, we will present an introduction on topological magnetic textures. Moreover, we will present methods to solve the LLG equations for some configurations. This theory will be fundamental for the understanding of the following chapters. In Chapter 3, we present the results

of the first published paper. We predict a periodic injection of domain walls in a nanowire by all electrical means. We study the stability of a certain magnetic configuration and derive a domain wall production for currents above a certain critical current. In Chapter 4, we present the results of the second published paper. We obtain a Hamiltonian formalism for the dynamical parameters that describe the current and magnetic field driven dynamics in ferromagnetic and antiferromagnetic nanowires. From this formalism, we obtain known results reported in the literature and predict new mechanisms, such as an orientation switch in an antiferromagnetic domain wall. In Chapter 5, we present the results of the third published paper. We extend the formalism of domain walls in nanowires to thin films. We describe how to obtain the dynamics of domain walls including local degrees of freedom along the wire. These are, for example, vortices and curvatures. Moreover, by considering closed domain walls, we describe the dynamics of smoothly deformed skyrmions in the large radius limit. We obtain the excitation modes of skyrmions. In the Conclusion, 6, we summarize all main results presented in the thesis.

2. METHODS

2.1 Micromagnetic model - the Landau-Lifshitz-Gilbert equation

The dynamical equations for the micromagnetic model is given by the Landau-Lifshitz-Gilbert (LLG) equation and it models a broad range of magnetic texture dynamics. It was initially proposed by Landau and Lifshitz to describe the motion of a system of magnetic moments under the influence of external magnetic fields. [25] The goal was to understand the ferromagnetic behavior of materials. Under the presence of an external magnetic field, ferromagnets tend to align with the applied field. For this reason, besides the energy conserving precessional movement of the magnetic moment, they introduced a phenomenological damping term to account for the alignment with the external field. Since this term could not account for more general dynamics observed in ferromagnets, Gilbert rederived the equations of motion for a system of magnetic moments using a variational approach. [37] The equation obtained was called LLG equation.

The starting point of this phenomenological theory is to describe the system of magnetic moments of a ferromagnet as a continuous magnetization vector field $\boldsymbol{M}(\boldsymbol{r})$ with constant magnitude,

$$|\boldsymbol{M}(\boldsymbol{r})| = M_s, \tag{2.1}$$

where M_s is the magnetization saturation, it correspond to the magnetization density of the material in the case where all magnetic moments are aligned, and $\boldsymbol{r}$ is the position of the local magnetization in the ferromagnet. The magnetic momentum of an electron is related to its spin momentum by

$$\boldsymbol{M} = -\gamma \boldsymbol{S}, \tag{2.2}$$

where $\gamma > 0$ is the gyromagnetic constant. A property of the spin momentum, is that it satisfies the SO(3) algebra

$$\{S_i, S_j\} = \epsilon_{ijk} S_k, \tag{2.3}$$

where S_i are the i-component of the spin momentum, $i = 1, 2, 3$, and ϵ_{ijk} is the skew-symmetric tensor in 3d. From the equation of motion for the dynamics of a spin angular momentum in the presence of a magnetic field $\boldsymbol{H}$ and a phenomenological damping term we obtain the intuitive[1] LLG equation, as seen on Ref. [37],

$$\frac{d\boldsymbol{M}}{dt} = -\gamma \boldsymbol{M} \times \boldsymbol{H} + \frac{\alpha}{M_s} \boldsymbol{M} \times \frac{d\boldsymbol{M}}{dt}, \tag{2.6}$$

where α is a dimensionless damping constant. The first term in Eq. 2.6 correspond to the precessional movement of the magnetization, while the second term, related to damping, aligns the magnetization with the external field, see Fig. 2.1. An important remark is that, it is preferable in many cases to study the dynamics of the magnetization orientation represented by the unitary vector $\boldsymbol{m} = \boldsymbol{M}/M_s{}^2$.

The magnetic field $\boldsymbol{H}$ felt by each magnetic moment may be due to external magnetic fields applied to the material as well as due to the surrounding magnetic moments. In the most general case, one can consider each magnetic moment in a "effective" magnetic energy potential $\mathcal{H}$ that takes into account all the interactions,

$$\boldsymbol{H} = -\frac{\delta \mathcal{H}}{\delta \boldsymbol{m}}. \tag{2.8}$$

---

[1]An important remark is that the LLG Eq. 2.6 can be obtained in a intuitive manner. From the fact that the magnetization vector $\boldsymbol{M}$ has constant magnitude, any variation of $\boldsymbol{M}$ must be perpendicular to $\boldsymbol{M}$,

$$d\boldsymbol{M} \perp \boldsymbol{M}. \tag{2.4}$$

Therefore we can always decompose the vectorial components of $d\boldsymbol{M}/dt$ into a basis orthogonal do $\boldsymbol{M}$,

$$\frac{d\boldsymbol{M}}{dt} = a_i \partial_i \boldsymbol{M} + \boldsymbol{M} \times \boldsymbol{b}, \tag{2.5}$$

where a_i and $\boldsymbol{b}_i$ are functions of $\boldsymbol{M}$ and other parameters of the systems. Therefore, by dimensional analysis and dynamical considerations, one can propose how each interaction contributes. This intuition will be important later to incorporate electrical current driven dynamics in the LLG equation.

[2]The LLG equation for the unitary vector field $\boldsymbol{m}$ is

$$\frac{d\boldsymbol{m}}{dt} = -\frac{\gamma}{M_s} \boldsymbol{m} \times \boldsymbol{H} + \alpha \boldsymbol{m} \times \frac{d\boldsymbol{m}}{dt}. \tag{2.7}$$

This will be the representation mostly used in this thesis.
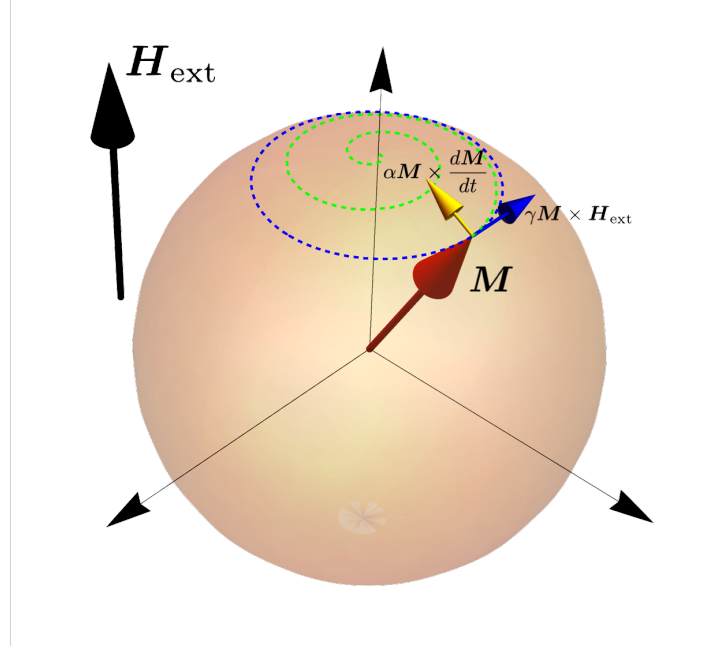
Figure 2.1: Representation of the LLG equation dynamics. The blue and yellow vectors represent the precessional force and the damping term respectively, they belong to a plane perpendicular to the magnetization direction M represented in red.. The blue circle corresponds to the precession movement caused by the external field. The green spiral is the final motion taking into account the damping.

Experimental observations and theoretical predictions have identified the main contributions for the effective Hamiltonian $\mathcal{H}$ as

$$\mathcal{H} = \mathcal{H}_{ex} + \mathcal{H}_{anys} + \mathcal{H}_{DMI} + \mathcal{H}_{dm} + \mathcal{H}_{\boldsymbol{H}_{ext}} + \mathcal{H}_{me}, \tag{2.9}$$

where $\mathcal{H}_{ex}$ is the exchange interaction, $\mathcal{H}_{anys}$ is the anysotropy energy, $\mathcal{H}_{DMI}$ is due to the Dzyaloshinskii-Moryia interaction (DMI), $\mathcal{H}_{dm}$ is the demagnetization energy, $\mathcal{H}_{H_{ext}}$ is the potential due to external magnetic fields and $\mathcal{H}_{me}$ is the magnetoelastic energy. $\mathcal{H}_{dm}$ and $\mathcal{H}_{H_{ext}}$ are due to actual magnetic fields while the other three potentials have quantum mechanical origins.

A brief description of the above interactions follows, for more details check references therein.

- The exchange energy, $\mathcal{H}_{ex}$, also called stiffness energy, is responsible in ferromagnetic systems for a constant equilibrium magnetization direction. This is one of the ferromagnetic
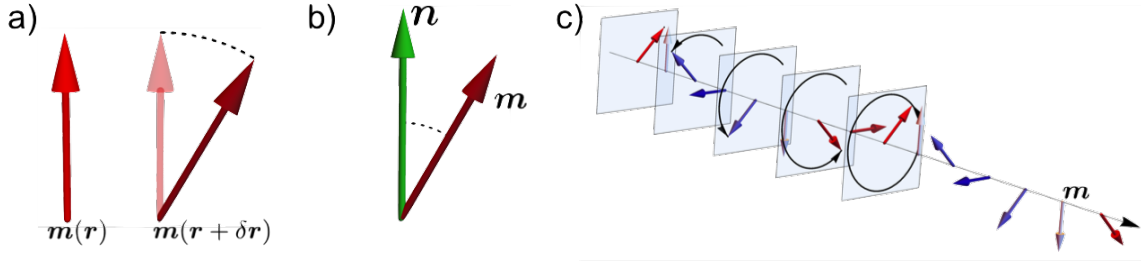
Figure 2.2: Representation some interactions between magnetic moments in a ferromagnet. Image a) correspond to the exchange interaction between neighboring magnetic moments as they tend to align. Figure b) correspond to anisotropy interaction with an easy axis, the magnetic moment tend to align with the easy axis given by $\boldsymbol{n}$. Figure c) correspond to a Bloch DMI that induces a rotation of the magnetization in a plane perpendicular to a certain direction.

material's most fundamental properties. It emerges from the interaction between nearest neighbors in the discrete lattice. It is proportional to the square of the gradient of the magnetization,

$$\mathcal{H}_{ex} = \frac{J}{2} \int dV (\boldsymbol{\nabla}\boldsymbol{m})^2, \tag{2.10}$$

where J is the exchange constant with dimension Energy/length. This constant depends on the properties of the material and in general changes with temperature. [38] If J is positive-valued, this interaction favor the alignment of all magnetic moments, this is called a ferromagnetic state, see Fig. 2.2 a). Negative values of J would favor a state with neighboring moments being in anti-parallel directions, this is called an antiferromagnetic state and the effective Hamiltonian is not applicable. The ground state for this interaction is invariant under a global rotation. This potential can be derived as a Taylor expansion of the Heisenberg interaction. [24]

- The anisotropy energy, $\mathcal{H}_{anys}$, is a potential that depends on the relative direction between the local magnetization and the structural axes of the material. The major contribution for this effective potential is the spin-orbit interaction. The function that describes the anisotropy energy is obtained by analyzing the symmetries of the material. In this thesis, we will only consider anisotropies with time reversal symmetry. Thus, only quadratic terms in the mag-

9

netization may appear,

$$\mathcal{H}_{anys} = \int dV \lambda \Pi \left((\boldsymbol{m} \cdot \boldsymbol{n})^2 \right) \tag{2.11}$$

where $\boldsymbol{n}$ is the direction defined by the material and λ is an overall constant to define the total strength of the anisotropy, i.e. $\Pi \left((\boldsymbol{m} \cdot \boldsymbol{n})^2 \right) = \pm 1$ at the maximum/minimum energy configurations. This potential is often expanded in a Taylor series. The signs of the expanded terms designate the preferred directions of the magnetization, for example the existence of an easy/hard axis, see Fig. 2.2 b). Due to symmetry it is also possible to obtain cubic anisotropy, among others, which favors more than one axis. [24]

- The DMI interaction, $\mathcal{H}_{DMI}$, are chiral interactions. It favors a rotation of the magnetization profile around a certain direction and with a defined chirality, see Fig. 2.2 c). It was first introduced by I. E. Dzyaloshinskii and T. Moryia in Refs. [39, 40]. The microscopic origins are spin-orbit scattering of electrons in inversion-asymmetric crystal fields. [41] Although this inversion asymmetry is absent in bulk structures, it plays an important role in multi-layered structures. The plane of rotation favored by DMI is given by structural aspects of the heterostructures. In general DMI can be classified as bulk (or Bloch DMI), $\mathcal{H}_{DMIB}$, and interfacial (or Néel DMI), $\mathcal{H}_{DMIN}$,

$$\mathcal{H}_{DMIB} = \int dV \left(-D_1(m_z \partial_x m_x - m_x \partial_x m_z) + D_2(m_z \partial_y m_y - m_y \partial_y m_z) \right), \tag{2.12a}$$

$$\mathcal{H}_{DMIN} = \int dV \left(D_1(m_z \partial_x m_x - m_x \partial_x m_z) + D_2(m_z \partial_y m_y - m_y \partial_y m_z) \right) \tag{2.12b}$$

where D_1 and D_2 are constants that depend on the symmetries of the chiral interaction and its strength. Different values for D_1 and D_2 are a recently discovered feature and are associated to the so called anisotropic DMI. [42]

- The demagnetization potential, $\mathcal{H}_{dm}$, is due to dipole-dipole interaction between the magnetic moments. It is a non-local interaction since it takes into account every single magnetic moment in the material. The reduced volume and surface charge densities, ρ and σ, respec-

tively, are given by

$$\rho = \boldsymbol{\nabla} \cdot \boldsymbol{m}, \quad \sigma = \boldsymbol{m} \cdot \boldsymbol{n}, \tag{2.13}$$

where $\boldsymbol{n}$ is the normal direction at the surface. The electrostatic potential created due to these charge densities is

$$\Phi_{elec}\boldsymbol{r}' = \frac{M_s}{4\pi\mu_0} \int dV \frac{\rho(\boldsymbol{r})}{|\boldsymbol{r}' - \boldsymbol{r}|} + \int dS \frac{\sigma(\boldsymbol{r})}{|\boldsymbol{r}' - \boldsymbol{r}|}, \tag{2.14}$$

where μ_0 is the vacuum magnetic permeability. Moreover, in terms of the charge densities and the electric potential, the total energy contribution from the dipole-dipole interaction is

$$\mathcal{H}_{dm} = \frac{M_s}{2} \left(\int dV \, \rho\Phi_{elec} + \int dS \, \sigma\Phi_{elec} \right). \tag{2.15}$$

This energy potential depends highly on the geometry of the magnetic structure and has relevant boundary effects. In lower dimensional structures, such as thin-films and nanowires, the above calculation can be simplified. In these cases, the demagnetization field can be seen as an effective easy-axis anisotropy with strength, [24, 43]

$$\lambda_{effect} = \frac{M_s^2}{2\mu_0}. \tag{2.16}$$

- The external field energy, $\mathcal{H}_{H_{ext}}$, also known as Zeeman energy, follow as the known interaction between the local magnetic moments $\boldsymbol{m}$ and an external field $\boldsymbol{H}_{ext}$

$$\mathcal{H}_{\boldsymbol{H}_{ext}} = -M_s \int dV \boldsymbol{H} \cdot \boldsymbol{m}. \tag{2.17}$$

- The magneto-elastic contribution, $\mathcal{H}_{me}$, emerges from the elastic degrees of freedom of magnetic crystals. Magnetic bodies deform under the influence of magnetic fields and this produces an energy potential. Since these effects are really small in ferromagnets, we will not take them into account in this thesis.

With the effective magnetic field, Eq. 2.8, given by the energy potentials in Eq. 2.9 and the LLG Eq. 2.7, it is possible to describe the magnetization dynamics in a broad range of materials. However, this rather non-local and non-linear complicated equation with infinite degrees of freedom often requires numerical calculations to obtain solutions. A method to simplify the micromagnetic equations is to reduce the number of degrees of freedom. The process of reducing the degrees of freedom is better understood from the underlying Hamiltonian and Lagrangian formalism of the LLG equation. For this reason, we will show how to obtain the LLG Eq. 2.7 from these formalisms.

2.1.1 Hamiltonian equation of motion

In the Hamiltonian formalism, the dynamics is described in terms of the phase space of generalized coordinates $\boldsymbol{q}$ and conjugated momenta $\boldsymbol{p}$ satisfying a Poisson bracket

$$\{q_\alpha, p_\beta\} = \delta_{\alpha\beta}, \tag{2.18}$$

where α, β are generalized indexes. The Hamiltonian equations of motion for the coordinates $\boldsymbol{q}, \boldsymbol{p}$ in terms of the Poisson bracket are

$$\frac{d\boldsymbol{q}}{dt} = \{\boldsymbol{q}, \mathcal{H}\} + \gamma_{\boldsymbol{q}}, \tag{2.19a}$$

$$\frac{d\boldsymbol{p}}{dt} = \{\boldsymbol{p}, \mathcal{H}\} + \gamma_{\boldsymbol{p}}, \tag{2.19b}$$

where $\mathcal{H}$ is the Hamiltonian for the system and $\gamma_{\boldsymbol{q},\boldsymbol{p}}$ are the damping terms.

For the dynamical system of magnetic moments $\boldsymbol{m}$, the Poisson bracket is given as in Eq. 2.3,

$$\{m_i(\boldsymbol{r}), m_j(\boldsymbol{r}')\} = -\frac{\gamma}{M_s}\epsilon_{ijk}m_k(\boldsymbol{r})\delta^3(\boldsymbol{r}' - \boldsymbol{r}). \tag{2.20}$$

The Hamiltonian is the one given in Eq. 2.9. The damping term, derived from a phenomenological viscosity term, is given by the Gilbert damping term $\alpha\boldsymbol{m} \times d\boldsymbol{m}/dt$. The LLG Eq. 2.7, therefore,

can be written as a Hamiltonian equation

$$\frac{d\boldsymbol{m}}{dt} = -\frac{\gamma}{M_s}\boldsymbol{m} \times \frac{\delta\mathcal{H}}{\delta\boldsymbol{m}} + \alpha\boldsymbol{m} \times \frac{d\boldsymbol{m}}{dt} \quad \leftrightarrow \quad \frac{d\boldsymbol{m}}{dt} = \{\boldsymbol{m}, \mathcal{H}\} + \gamma_{\boldsymbol{m}}. \tag{2.21}$$

2.1.2 Lagrangian Formalism and Berry phase

The Lagrangian formalism obtains the equations of motion from an action functional $\mathcal{A}[\boldsymbol{m}]$,

$$\mathcal{A}[\boldsymbol{m}] \equiv \int dt \mathcal{L}[\boldsymbol{m}], \tag{2.22}$$

where $\mathcal{L}[\boldsymbol{m}]$ is called a Lagrangian and is a functional of the magnetic configuration $\boldsymbol{m}$. By using the variational principle, the equations of motion correspond to the Euler-Lagrange equation,

$$\frac{d}{dt}\left(\frac{\delta\mathcal{L}[\boldsymbol{m}]}{\delta d\boldsymbol{m}/dt}\right) - \frac{\delta\mathcal{L}[\boldsymbol{m}]}{\delta\boldsymbol{m}} = 0. \tag{2.23}$$

A difficulty of to obtain the Lagrangian formalism for the magnetic moment field dynamics is the unusual Poisson bracket in Eq. 2.20. From the constraint of the constant magnitude, it is known that not all degrees of freedom of $\boldsymbol{m}$ are independent. Furthermore, from the structure of the Poisson bracket in Eq. 2.20 one obtains that these degrees of freedom are dynamically conjugated. The kinetic part of the Lagrangian $\mathcal{L}[\boldsymbol{m}]$, i.e. dependent of $d\boldsymbol{m}/dt$, is given by the spin Berry phase. [44] In the reference frame of the magnetic moment, the adiabatic time evolution is associated to a geometrical phase given by

$$\gamma_t = \boldsymbol{A} \cdot \frac{d\boldsymbol{m}}{dt}, \tag{2.24}$$

where $\boldsymbol{A}[\boldsymbol{m}]$ is the gauge potential of a magnetic monopole with field strength

$$\sum_{jk}\epsilon_{ijk}\frac{\delta A_j}{\delta m_k} = -\frac{M_s}{\gamma}m_i. \tag{2.25}$$

13

This gauge potential is invariant under gauge transformations [3]. Once the magnetization completes a cycle, the area covered by the spin correspond to the Berry phase[4]

$$\mathcal{S}_B = \int dt\, \boldsymbol{A} \cdot \frac{d\boldsymbol{m}}{dt}, \tag{2.28}$$

see Fig. 2.3.
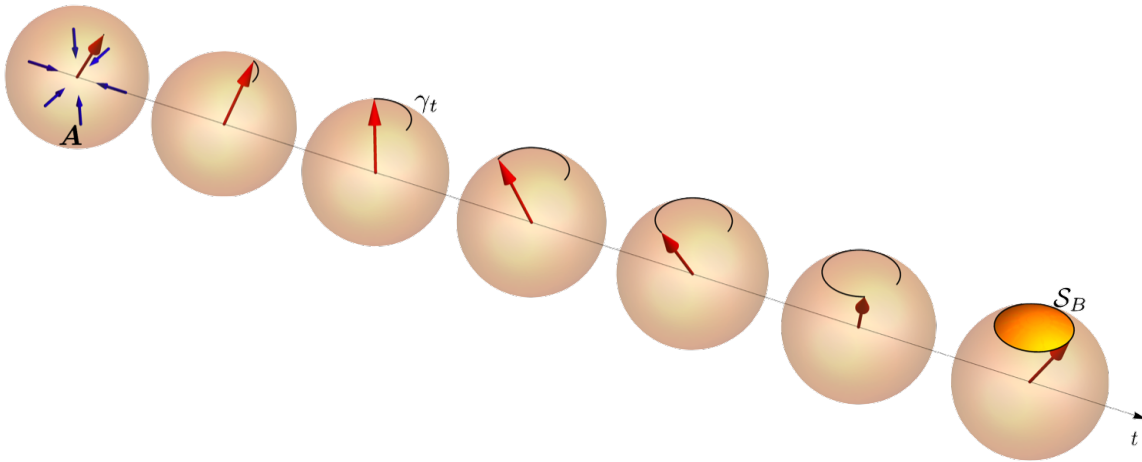
Figure 2.3: Representation of the spin Berry phase. On the first sphere in the left, we show the magnetic moment $\boldsymbol{m}$ in the presence of the field potential $\boldsymbol{A}$. As it evolves in time, it acquires a phase given by γ_t. In the last panel we see the cap representing the spin Berry phase.

The Action given by the Berry phase, Eq. 2.28, and the Hamiltonian, Eq. 2.9,

$$\mathcal{A} = \mathcal{S}_B - \int dt\mathcal{H}, \tag{2.29}$$

---

[3]A common representation of the gauge potential, $\boldsymbol{A}[\boldsymbol{m}]$, is

$$\boldsymbol{A} = \frac{M_s}{\gamma} \frac{\boldsymbol{e}_z \times \boldsymbol{m}}{1 - \boldsymbol{e}_z \cdot \boldsymbol{m}}, \tag{2.26}$$

as seen in Ref. [45].

[4]In the spherical representation, $\boldsymbol{m} = (\sin\theta\cos\phi, \sin\theta\sin\phi, \cos\theta)$, the potential in Eq. 2.26 becomes the usual representation of the Berry phase

$$\mathcal{S}_B = \frac{M_s}{\gamma} \int dt\, (\cos\theta - 1) \frac{d\phi}{dt}. \tag{2.27}$$

provides the energy conserving dynamics, i.e. the precessional movement of the magnetic moment, of the LLG Eq. 2.7.

To obtain the damping factor, one needs to include the presence of a dissipative force to the equation of motion, i.e. a force proportional to the time evolution. This can be done by adding a term to the Euler-Lagrange equation of motion 2.23,

$$\frac{d}{dt}\left(\frac{\delta\mathcal{L}[\boldsymbol{m}]}{\delta d\boldsymbol{m}/dt}\right) - \frac{\delta\mathcal{L}[\boldsymbol{m}]}{\delta\boldsymbol{m}} + \frac{\delta\mathcal{R}}{\delta d\boldsymbol{m}/dt} = 0, \tag{2.30}$$

where

$$\mathcal{R}\left[\frac{d\boldsymbol{m}}{dt}\right] = \frac{\alpha M_s}{2\gamma}\int dV\left(\frac{d\boldsymbol{m}}{dt}\right)^2 \tag{2.31}$$

is the Rayleigh dissipation functional, see Ref. [37].

2.1.3 Torque due to currents

So far, in the LLG equation, we only included interaction between the local magnetic moments in the lattice. It is possible, however, to add an interaction with itinerant spins in the lattice. They correspond to free electrons moving in the ferromagnet. For a reading on the theory that models ferromagnetic materials as composed by fixed local magnetizations and free electrons, we suggest Ref. [46]. Electrons are endowed with an electric charge and a spin degree of freedom. The spin of an electron can interact with the local magnetization through mostly two ways: spin transfer torque (STT) and spin orbit torque (SOT). In this work we will focus on spin transfer torque. For these interactions, we need to consider not the current of electric charge, but of the spin momentum of the electron. STT is due to the change in the spin moment of the electron as it moves around a magnetic configuration, see Fig. 2.4, while SOT is due to interaction between the spin momentum and the local magnetic moment. The relation between the spin polarized current, v_s, and the electric current, j, is given by

$$v_s = \frac{jP\gamma\hbar}{2eM_s}, \tag{2.32}$$

where P is the polarization rate, i.e. the rate of spins aligned in the electric current, and e is the electric charge. [47]
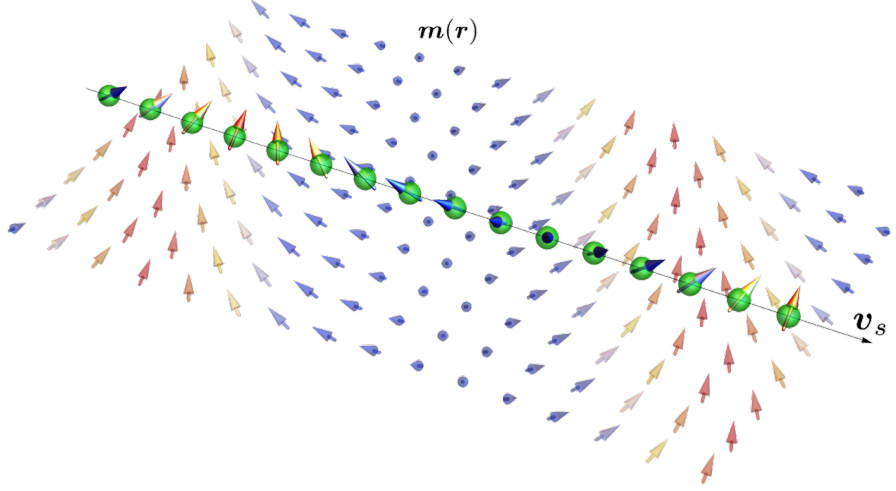
Figure 2.4: Representation of a spin current, v_s, flowing in a magnetic texture m. Notice that the spin current aligns with the local magnetization.

For the adiabatic motion of the spin current, we can consider the spin transfer torque as the limit for infinitely thin successive cross-sections of the Slonczewski spin transfer term, [48, 49, 50],

$$\frac{d\boldsymbol{m}}{dt} = -(\boldsymbol{v}_s \cdot \boldsymbol{\nabla})\boldsymbol{m}. \tag{2.33}$$

This interaction can be obtained by an associated Berry phase gain for the electron. As the spin of the electron follows the magnetization orientation, the spin precesses and the electron acquires a Berry phase. In the spherical representation for the spin of the electron,

$$\mathcal{S}_{B\,e} = -\int dt \, (\cos\theta - 1) \, (\boldsymbol{v}_s \cdot \boldsymbol{\nabla})\phi. \tag{2.34}$$

Another interpretation for the origin of the adiabatic STT is called the spin valve. As a spin currents

passes through a region with constant magnetic moment orientation, the spins are "filtered". This produces a torque in the magnetization. The accumulation of magnetic moment, however, can lead to another torque. It is called non-adiabatic torque. It is perpendicular to the adiabatic torque. This interaction that results from non-equilibrium states is associated to a damping term, [50],

$$\frac{d\boldsymbol{m}}{dt} = -\beta\boldsymbol{m} \times ((\boldsymbol{v}_s \cdot \boldsymbol{\nabla})\boldsymbol{m}), \tag{2.35}$$

where β is a positive constant determined phenomenologically.[5]

2.1.4 Antiferromagnets

For a broader application of spintronics, we need to consider also antiferromagnets. Antiferromagnets are associated to neighboring magnetic moments being anti-parallel, i.e. a negative exchange constant. This means that the total magnetic moment is zero. In these materials there is no stray field and they are insensitive to external magnetic fields. [51] These features present both advantages and obstacles. On one hand, it allows for a more efficient spin dynamics. Textures are more sensitive to electric currents. On the other hand, the magnetic invisibility makes it difficult to detect and manipulate magnetic textures. Overall, the field of antiferromagnetic spintronics has seen a lot of progress recently in experimental techniques. [52, 53, 54, 55, 56, 57]

From a macroscopic point of view, in order to allow for a good description of the sum of the magnetic moment of neighboring atoms being zero, AFM materials are often described as a system of interleaved magnetic sublattices. [58] A particular case are bipartite lattices, in which one consider only two ferromagnetic sublattices described by $\boldsymbol{m}_A(\boldsymbol{r})$ and $\boldsymbol{m}_B(\boldsymbol{r})$, see Fig. 2.5. In this model, one defines the Néel vector as $\boldsymbol{l} = \boldsymbol{m}_A - \boldsymbol{m}_B$ and the AFM magnetization vector $\boldsymbol{M} = \boldsymbol{m}_A + \boldsymbol{m}_B$. The AFM nature is realized by a strong exchange interaction between lattices

---

[5]From a intuitive point of view, the above dependences for the spin transfer torques are unique. Assuming that the spin momentum of the electron couples with the variation of the magnetization, $(\boldsymbol{v}_s \cdot \boldsymbol{\nabla})\boldsymbol{m}$, and a proper choice for a basis for these interactions, see Eq. 2.5, the total torque due to electric current must be

$$\frac{d\boldsymbol{m}}{dt} \propto a(\boldsymbol{j} \cdot \boldsymbol{\nabla})\boldsymbol{m} + b\,\boldsymbol{m} \times ((\boldsymbol{j} \cdot \boldsymbol{\nabla})\boldsymbol{m}), \tag{2.36}$$

where the constants a and b can be chosen to fit the theory from a phenomenological point of view.
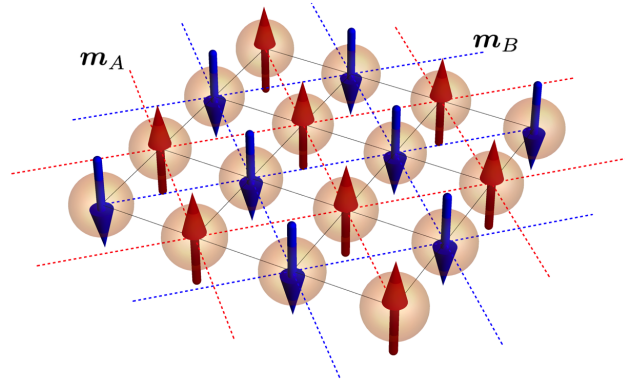
Figure 2.5: Schematics of an antiferromagnetic bipartite lattice. The black lines shows the next neighbors, the red lines and blue lines shows the decomposition of the lattice into two sublattices, $\boldsymbol{m}_A$ and $\boldsymbol{m}_B$, respectively.

favoring a configuration for which $M \to 0$. This decomposition into ferromagnetic sublattices will be the basis of the description of topological textures in AFM structures in this work.

2.2 Topological magnetic textures

Topological magnetic textures are smooth magnetic field configurations on a surface that are homotopically different from the ferromagnetic state. This usually occurs when the boundary conditions for the surface allows for non-trivial homotopy groups. Due to the topological properties, there are no smooth transformation that allows to obtain the ferromagnetic state from the topologically non-trivial configuration state. This property grants them stability. For real materials, in which one needs to take into account the discretization of the lattice, these states usually correspond to local minima of the energy functional and are stable or metastable states. [21, 59, 60] The non-trivial topological configurations arise mainly from interactions that allows for a twist of the magnetization, see Fig. 2.6. Dipole-dipole interactions and DMI induce a continuous twisting and generates a sequence of different magnetization orientations. Anisotropy interactions, which induces a discrete symmetry for the ground states, also allows for the formation of topological

structures with the coexistence of different domains in the same structure.

This thesis will focus on field configurations in one and two dimensional structures. In one dimension one observe the existence of domain walls. In two dimensions a much richer range of possibilities is possible. We will focus on extended domain walls and skyrmions. In the next subsections we will present the basic ideas of these topological solutions.
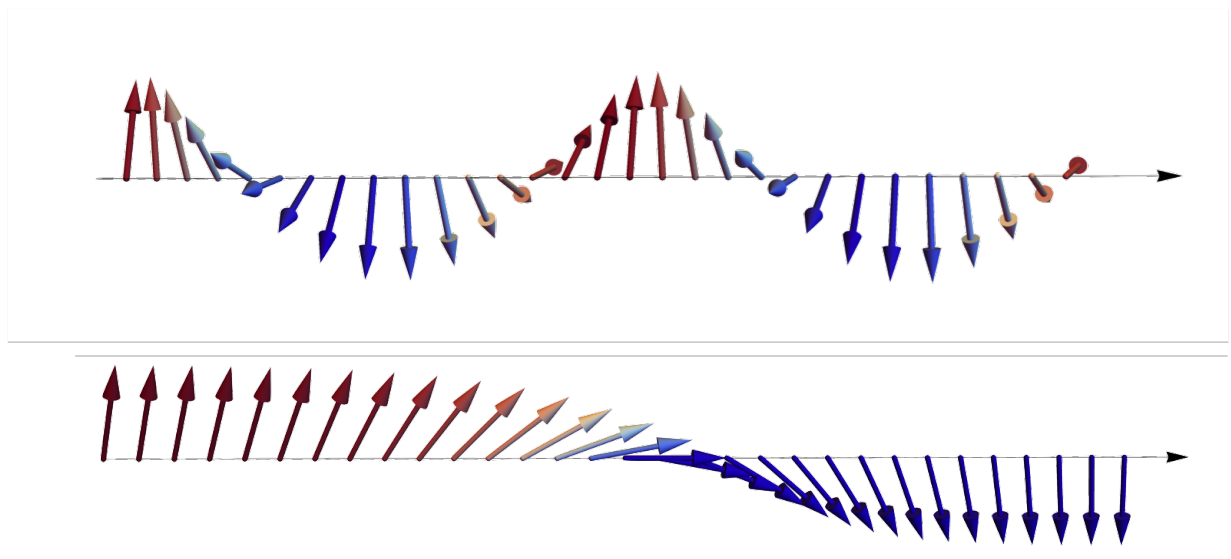
Figure 2.6: Existence of non-trivial magnetic configurations due to (a) twisting interactions and (b) anisotropy interaction

2.2.1 Domain walls

Domain walls (DW) correspond to the finite-sized transition between two inequivalent ferromagnetic states. Usually one observes $180°$ and $90°$ DWs, associated to easy-axis anisotropy or shape anisotropies. [24] In this thesis we will only consider the first. The name "domain wall" comes from the idea of domains. In magnetism, domain is a region where all magnetic moments are aligned, i.e. in the ferromagnetic state. Exchange interaction, external magnetic fields and easy axis anisotropies favors the formations of domains. The coexistence of different domains in the same sample is associated to domain walls on the boundary between these domains.

The topological properties of a DW may be understood from the idea of identifying opposite ends of a thin ribbon. In the presence of a a unique ferromagnetic state, it is possible to identify the structure with ends identified to a loop. In the presence of a DW, to identify opposite ends of the ribbon, one requires a twist of the ribbon. This generates what is called a Möbius strip. A Möbius strip is topologically inequivalent to a loop, see Fig. 2.7. From the energy point of view, the stability of the DW state is due to being a local minima. In order to go from a DW state with two domains to a single domain, it is necessary to flip a macroscopic number of magnetic moments.
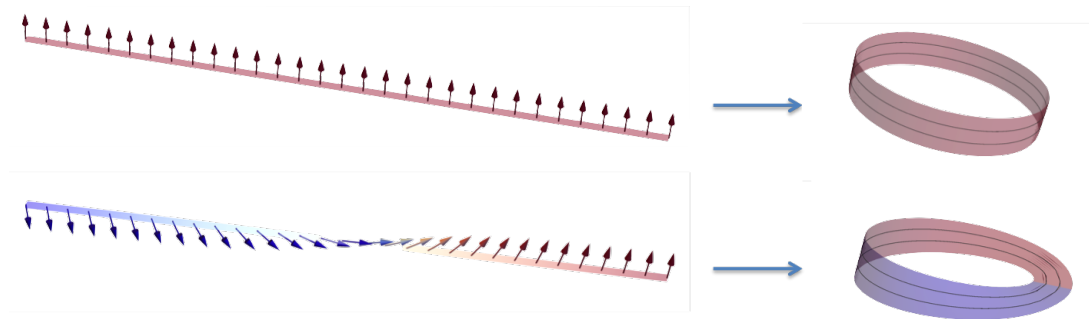
Figure 2.7: Representation of topology properties of DWs. If one identify the ends of a strip in the ferromagnetic state we obtain a loop, while if we do the same procedure for a DW, we obtain a Möbius strip.

According to the plane of rotation of the magnetic moments in a DW, it can be named as a Bloch DW, in which the plane of rotation is perpendicular to the transition, and as Néel DW, in which the plane of rotation is along the transition, see Fig. 2.8.

The simplest solution for a DW is given by a model with only exchange interaction and easy-axis anisotropy. This solution provides a natural length and energy scales for the magnetization textures. Given a nanowire along the x-axis, with an easy axis along an $\hat{e}_z$ orientation, we obtain
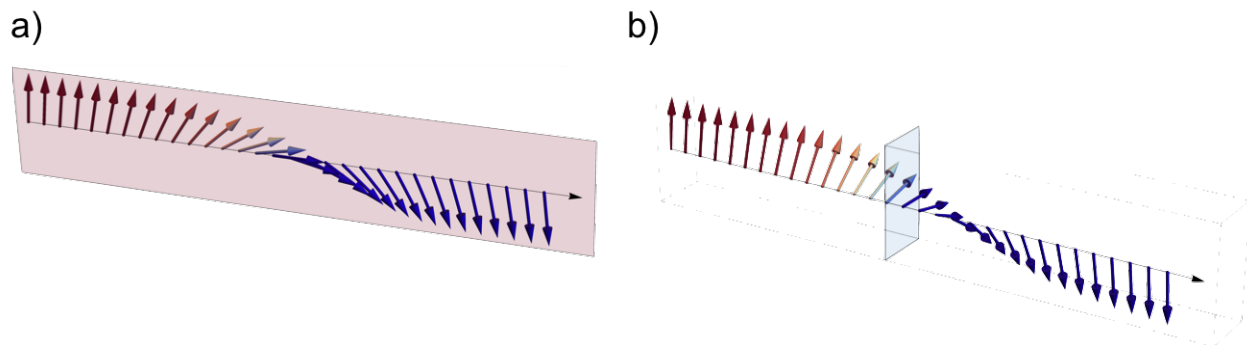
Figure 2.8: Representation (a) Néel DW, the magnetization rotates within the DW plane; (b)Bloch DW, the magnetization rotates in a plane perpendicular to the DW plane.

an effective Hamiltonian density, $\mathcal{H}$, of the form

$$\mathcal{H} = \int dx \left(\frac{J}{2} \left(\partial_x \boldsymbol{m} \right)^2 - \lambda m_z^2 \right), \tag{2.37}$$

where J is the positive exchange constant and λ is the positive anisotropy constant. A natural rescaling parameter is $x \to \tilde{x} = x/\Delta$, where $\Delta = \sqrt{J/2\lambda}$. Notice that $\tilde{x}$ is dimensionless. The Hamiltonian density from Eq. 2.38 becomes

$$\mathcal{H} = \mathcal{E}_{DW} \int d\tilde{x} \left(\left(\partial_{\tilde{x}} \boldsymbol{m} \right)^2 - m_z^2 \right), \tag{2.38}$$

where $\mathcal{E}_{DW} = \sqrt{JK/2}$ is the DW energy density. [24] The states with minimum energy are the two opposite ferromagnetic states, $\boldsymbol{m} = \pm \hat{\boldsymbol{e}}_z$. The DW solution corresponds to state with minimum energy satisfying the boundary conditions $\boldsymbol{m} = \hat{\boldsymbol{e}}_z$ at one end and $\boldsymbol{m} = -\hat{\boldsymbol{e}}_z$ at the other end. To perform this calculation, it is helpful to consider the $\boldsymbol{m}$ in the spherical representation,

$$\boldsymbol{m} = \left(\sin\theta\cos\phi, \sin\theta\sin\phi, \cos\theta \right). \tag{2.39}$$

In this representation, Eq. 2.38 becomes

$$\mathcal{H} = \mathcal{E}_{DW} \int d\tilde{x} \left((\partial_{\tilde{x}}\theta)^2 + \sin^2\theta \, (\partial_{\tilde{x}}\phi)^2 - \cos^2\theta \right). \tag{2.40}$$

The minimization of this effective energy is given by the following equations

$$\partial_{\tilde{x}} \left(\sin^2\theta \partial_{\tilde{x}}\phi \right) = 0, \tag{2.41a}$$

$$\partial_{\tilde{x}}^2 \theta - \sin 2\theta \left((\partial_{\tilde{x}}\phi)^2 + 1 \right) = 0 \tag{2.41b}$$

The solution for both equations with the boundary conditions $\theta_{+\infty} = -\theta_{-\infty}$, where $\theta_{-\infty} = \pm\pi/2$, are

$$\phi = \phi_0, \quad \sin\theta = \tanh\left(\frac{x + x_0}{\Delta} \right). \tag{2.42}$$

where ϕ_0 and x_0 are constants. Notice that this solution is invariant under a global rotation of ϕ and the profile is invariant under a translation along x, typical of a translationally invariant Hamiltonian. For more general solutions of DWs, check Ref. [24]. The dynamics of DWs will be presented in following sections.

2.2.2 Skyrmions

Magnetic skyrmions are topological objects in two dimensions. The mathematical definition of a Skyrmion is: *a smooth field configuration defined by a non-trivial surjective map from the coordinate space, corresponding to the thin-film $\mathbb{R}^2$, to an order parameter space, a spherical shell S^2, with a non-trivial topology.* It is everywhere non-singular, finite and with no winding number at infinity. In other words, if one considers a unitary smooth vectorial field, $\boldsymbol{m}$, on an infinite plane with the orientation at infinity identified, it is possible to associate the vectorial field to a covering of a sphere. The solid-angle, Ω, corresponding to this cover is given by

$$\Omega = \int d^2x \, \boldsymbol{m} \cdot (\partial_x \boldsymbol{m} \times \partial_y \boldsymbol{m}). \tag{2.43}$$

It is possible to collapse into a single point, corresponding to the orientation at infinity, through a smooth transformation any partial cover of the sphere. However, a complete cover of the sphere can not collapse into a single point through smooth transformations, see Fig. 2.9. Therefore, the covering of a sphere corresponds to a topological property. A skyrmion corresponds to each time the field configuration cover the sphere. We associate to it the integer topological charge

$$Q = \frac{1}{4\pi} \int d^2x \, \boldsymbol{m} \cdot (\partial_x \boldsymbol{m} \times \partial_y \boldsymbol{m}) \,, \tag{2.44}$$

which is also called *winding number*.
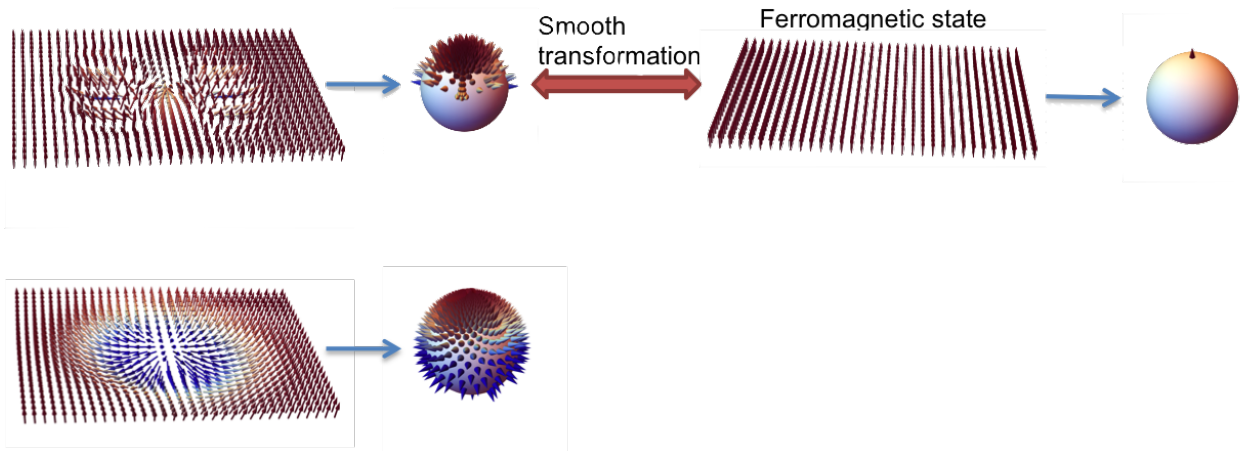
Figure 2.9: A sketch between the magnetic configurations on a plane and the projection to a sphere. Notice that while configuration that cover partially the sphere can collapse to the ferromagnetic state, skyrmions are not allowed to by smooth transformations.

The existence of magnetic skyrmions was shown by Bogdanov and collaborators in the late 1980's and early 1990's as mean-field ground states for models of anisotropic, non-centrosymmetric magnetic materials with chiral spin-orbit interactions subjected to an applied magnetic field. [30, 31, 61] Their existence were previously mentioned by Pokrovsky in 1978. [62] Skyrmions were experimentally observed by the first time as a skyrmion-tube lattice in the cubic helimagnet manganese silicide (MnSi) in the presence of an applied external magnetic field. [32] Beyond skyrmion

lattices, other skyrmion textures have been discussed in thin films such as magnetic bubble domains. [63] Skyrmion configurations emerge from the interplay between three hierarchical energy scales: ferromagnetic exchange coupling, crystalline field interactions and twisting interactions (such as DMI and dipole-dipole interactions). The latest interaction defines the typical size of skyrmions, ranging from $100\text{nm} - 1\mu\text{m}$, in the case of long range dipole-dipole interactions, and $5 - 100\text{nm}$ in the case of DMI. For a general discussion of skyrmions we recommend Ref. [15].

The magnetic profile of a skyrmion is highly dependent on its size. [24, 31, 64] In this thesis we will focus on skyrmions with radius much larger than the DW width. In this case, the skyrmion can be considered as closed DWs. [3, 59] In the same sense as in the DW, a skyrmion may classified as a Bloch skyrmion or Néel skyrmion if the closed DW that defines the radius of the skyrmion is a Bloch or Néel DW.

2.3 Methods to study magnetization dynamics

The dynamics of the magnetic moments in a ferromagnet is well described by the LLG Eq. 2.7. This equation is highly non-linear, non-local and with infinite degrees of freedom. These conditions impose a major challenge for full analytical solutions and often requires numerical calculations.

Numerical calculations are often performed by micromagnetic simulation softwares, e.g. MuMax3, [65], and MicroMagnum, [66]. These softwares use the LLG equation to calculate consecutive configurations of a discretized magnetic sample. Given an initial configuration and the desired perturbations, the simulations provide the corresponding time evolution of the configuration. These simulations are extremely useful to provide the expected behavior in experiments for a broad range of situations.

For the analytical calculations, a way to overcome the challenges imposed by the model is to consider simplifications of the LLG equation. There are two important methods: linearization and soft mode description. The linearization of the LLG equations allows for studying small perturbations of an static state. This method is largely used to study the excitation modes of the ferromagnetic state and other magnetic configurations. [4, 67, 68] It is also the basis for the analytical studies

24

of spin waves. Spin waves are propagating perturbations of the local magnetic state. [69, 70] Their great advantage is that they can carry information without moving charges, and therefore avoid Joule heating. Their range of frequencies are in the GHz and low THz regime. The soft mode description is another largely used method to solve the dynamical LLG equation is the soft mode approach. Due to the stability of topological magnetic textures, their low energy excitation modes are described by a reduced number of degrees of freedom. [35, 71] This allows for the description of dynamics of topological textures via a finite number of time dependent parameters and their equations of motion.

In this section we will briefly introduce two methods used to study analytically the magnetization dynamics: 1) Linearization, and 2) Soft mode description.

2.3.1 Linearization and spin waves

This method is based on considering small perturbations, $\boldsymbol{s}$, of well defined magnetic configurations, $\boldsymbol{m}_s$. The major feature of the method is that it produces a linear equation of motion for the perturbation $\boldsymbol{s}$. First, we consider a total magnetization field, $\boldsymbol{m}_T$, given by

$$\boldsymbol{m}_T = \boldsymbol{m}_s + \boldsymbol{s}, \tag{2.45}$$

where $\boldsymbol{m}_s$ is a solution of the LLG equation under some specific conditions and $\boldsymbol{s}$ is a small perturbation around the solution $\boldsymbol{m}_s$. The condition for the magnitude of $\boldsymbol{s}$ is that it is much smaller than 1, $|\boldsymbol{s}| \ll 1$. The magnitude of $\boldsymbol{m}_T$ and $\boldsymbol{m}_s$, both solutions to the LLG equation, must satisfy, however, the unit magnitude constraint, $|\boldsymbol{m}| = 1$. A simple calculation reveals that $\boldsymbol{s} \perp \boldsymbol{m}_s$,

$$(\boldsymbol{m}_s + \boldsymbol{s}) \cdot (\boldsymbol{m}_s + \boldsymbol{s}) = \boldsymbol{m}_T \cdot \boldsymbol{m}_T$$

$$|\boldsymbol{m}_s|^2 + |\boldsymbol{s}|^2 + 2\boldsymbol{m}_s \cdot \boldsymbol{s} = 1$$

$$1 + 2\boldsymbol{m}_s \cdot \boldsymbol{s} \approx 1$$

$$\boldsymbol{m}_s \cdot \boldsymbol{s} \approx 0, \tag{2.46}$$

where we used that $|s|^2 \ll 1$. For this reason, it is possible to decompose s in a basis on the plane perpendicular to m_s, see Fig. 2.10. Usually, given a magnetization m_s, a natural basis on the
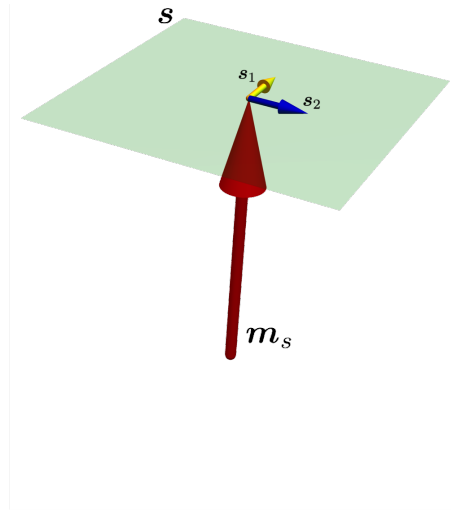
Figure 2.10: Representation of the magnetization m_s and the plane that must contain the perturbation $\vec{s}$. $s_{1,2}$ represent a basis on the plane.

plane orthogonal to the unitary vector m_s is given by δm_s and $m \times \delta m_s$. For m_s in the spherical coordinate representation,

$$m_s = (\sin\theta_s \cos\phi_s, \sin\theta_s \sin\phi_s, \cos\theta_s), \tag{2.47}$$

we consider usually a basis using the variation $\delta m_s \to \partial_{\theta_s} m_s$. The procedure above provides the following basis to study the perturbations of a state m_s, [4, 5, 72],

$$\hat{e}_1 \equiv m_s = (\sin\theta_s \cos\phi_s, \sin\theta_s \sin\phi_s, \cos\theta_s) \tag{2.48a}$$

$$\hat{e}_2 = (\cos\theta_s \cos\phi_s, \cos\theta_s \sin\phi_s, -\sin\theta_s), \tag{2.48b}$$

$$\hat{e}_3 = (-\sin\phi_s, \cos\phi_s, 0). \tag{2.48c}$$

With this basis, the perturbation s can be decomposed as

$$s = s_1 \hat{e}_2 + s_2 \hat{e}_3. \tag{2.49}$$

Furthermore, the total magnetization, m_T, is given by

$$m_T = \hat{e}_1 \sqrt{(1 - s_1^2 - s_2^2)} + s_1 \hat{e}_2 + s_2 \hat{e}_3, \tag{2.50}$$

which satisfies the unitary constraint, $|m_T| = 1$. In some cases, it is also possible to consider a complex plane given by

$$\hat{e}_\pm = \frac{1}{\sqrt{2}} \left(\hat{e}_2 \pm i \hat{e}_3 \right). \tag{2.51}$$

In this case, the total magnetization definition 2.50 becomes

$$m_T = \hat{e}_1 \sqrt{1 - 2\eta \, \eta^*} + \eta \hat{e}_+ + \eta^* \hat{e}_-. \tag{2.52}$$

Since $\hat{e}_1$ satisfies the LLG Eq. 2.7,

$$\frac{d\hat{e}_1}{dt} = -\frac{\gamma}{M_s} \hat{e}_1 \times H[\hat{e}_1] + \alpha \hat{e}_1 \times \frac{d\hat{e}_1}{dt}, \tag{2.53}$$

and we can expand the dynamical equation for the total magnetization, m_T, up to linear order in the perturbations. Or, equivalently for the dynamics without damping terms, consider the Lagrangian up to the quadratic order in the perturbations. [4, 5, 49, 73, 74, 75]

The method described above is often used to obtain the dispersion relations for spin waves and the energy excitations of topological textures. [68, 72, 76] For the latter, however, the complicated potentials usually requires sophisticate numerical calculations.

As a quick example of the linearization method, we will calculate the spin wave dispersion of the ferromagnetic state in ferromagnetic thin-film with easy-axis anisotropy. In this case, the

effective Hamiltonian 2.9 reduces to

$$\mathcal{H} = \tau \int d^2x \left(\frac{J}{2} (\boldsymbol{\nabla m})^2 - \lambda m_z^2 \right).$$ (2.54)

For $D < 4\mathcal{E}_{DW}/\pi$, the ground state is given by the ferromagnetic state $\boldsymbol{m} = \pm\hat{\boldsymbol{e}}_z$. It is important to remark that for $D > 4\mathcal{E}_{DW}/\pi$ the ground state correspond to helical states that may contain skyrmion lattices. [30, 32, 59] The equation of motion for a perturbation of the ferromagnetic ground state in this case is given by

$$\frac{d\boldsymbol{s}}{dt} = \frac{\gamma}{M_s} \hat{\boldsymbol{e}}_z \times \left(J\boldsymbol{\nabla}^2 \boldsymbol{s} - 2\lambda\boldsymbol{s} \right).$$ (2.55)

By considering that the perturbations assume can be decomposed in a basis of wave equations, corresponding to spin waves, we obtain the following dispersion relation

$$\omega = \frac{\gamma}{M_s} \left(J\boldsymbol{k}^2 + 2\lambda \right)$$ (2.56)

where $\boldsymbol{k}$ is the wave vector. [5] Notice that there is an activation gap, $2\lambda\gamma/M_s$, due to the presence of anisotropy.

2.3.2   Soft mode approach

The infinite degrees of the LLG Eq. 2.7 written in terms of $\boldsymbol{m}(\boldsymbol{r},t)$ can be mapped to equations in terms of an infinite set of dynamical parameters, $\boldsymbol{\xi}(t)$,

$$\boldsymbol{m}(\boldsymbol{r},t) \equiv \boldsymbol{m}(\boldsymbol{r}, \{\boldsymbol{\xi}(t)\}).$$ (2.57)

This method is called *collective coordinate* approach and it is valid for the most general case. [35] A remark is that this description is model independent. From a macroscopic point of view, the possibility of classify the dynamical parameters in different time scales allows for the study of certain specific behaviors of the magnetization by analyzing solely the equations of motions for a

finite set of parameters.

The time evolution of the magnetic field, $\boldsymbol{m}$, in terms of the dynamical parameters, $\boldsymbol{\xi}(t)$ is given by

$$\dot{\boldsymbol{m}}(\boldsymbol{r},t) = \sum_{\boldsymbol{\xi}_i} \dot{\boldsymbol{\xi}}_i \partial_{\boldsymbol{\xi}_i} \boldsymbol{m}, \tag{2.58}$$

where, from now on, for any function $f(t)$, $df/dt = \dot{f}$. Performing this substitution into the LLG Eq. 2.7, multiplying by $(\boldsymbol{m} \times \partial_{\boldsymbol{\xi}_i} \boldsymbol{m})$, and integrating over the whole volume of the structure provide a generalization of Thiele's equations [35, 71, 77]

$$\sum_j G_{ij} \dot{\boldsymbol{\xi}}_j = \frac{\gamma}{M_s} \frac{\partial \mathcal{H}}{\partial \boldsymbol{\xi}_i} + \alpha \sum_j \mathcal{D}_{ij} \dot{\boldsymbol{\xi}}_j \tag{2.59}$$

where the matrix elements G_{ij} and $\mathcal{D}_{ij}$ are

$$G_{ij}[\boldsymbol{\xi}] = \int dV \, \boldsymbol{m} \cdot \left(\partial_{\boldsymbol{\xi}_i} \boldsymbol{m} \times \partial_{\boldsymbol{\xi}_j} \boldsymbol{m} \right), \tag{2.60a}$$

$$\mathcal{D}_{ij}[\boldsymbol{\xi}] = \int dV \left(\partial_{\boldsymbol{\xi}_i} \boldsymbol{m} \cdot \partial_{\boldsymbol{\xi}_j} \boldsymbol{m} \right), \tag{2.60b}$$

and are called the gyrotropic tensor and the viscosity tensor respectively. In the formalism of collective coordinates we map the LLG equation with infinite degrees of freedom to an infinite set of Eqs. 2.59 to for the dynamical parameters. It is important to remark that, as seen in Eq. 2.21, the Thiele equations also correspond to a Hamiltonian equation,

$$\dot{\xi}_i = \{\xi_i, H\}_{\boldsymbol{q},\boldsymbol{p}} + \gamma_{\xi_i}, \tag{2.61}$$

where the Poisson brackets $\{\cdot,\cdot\}_{\boldsymbol{q},\boldsymbol{p}}$ are now defined for pairs of canonical variables $(\boldsymbol{q}_i, \boldsymbol{p}_i)$ in terms of the independent collective coordinates $\boldsymbol{\xi}_i(t)$ and their time derivatives $\dot{\boldsymbol{\xi}}_i(t)$. The definition of $(\boldsymbol{q}_i, \boldsymbol{p}_i)$ follows from the spin Berry phase defined in Eq. 2.28. Using the substitution 2.58 in Eq. 2.28, one obtains

$$\mathcal{S}_B = \frac{M_s}{\gamma} \int dt \dot{\boldsymbol{\xi}}_i \sum_{\boldsymbol{\xi}_i} \int dV \, \boldsymbol{A} \cdot \partial_{\boldsymbol{\xi}_i} \boldsymbol{m}, \tag{2.62}$$

29

so that we can write $\boldsymbol{q}_i \to \boldsymbol{\xi}_i$ and $\boldsymbol{p}_i \to \int dV \, \boldsymbol{A} \partial_{\boldsymbol{\xi}_i} \boldsymbol{m}$. Since $\boldsymbol{A}$ is a function of $\boldsymbol{m}$ which depends only on the set of dynamical parameters $\boldsymbol{\xi}_i$, it is clear that $\boldsymbol{p}_i$ can also be written in terms of the dynamical parameters $\boldsymbol{\xi}_i$. If we take the derivative of $\boldsymbol{p}_i$ in terms of $\boldsymbol{\xi}_j$ we obtain

$$
\begin{aligned}
\partial_{\boldsymbol{\xi}_j} \int dV \, \boldsymbol{A} \cdot \partial_{\boldsymbol{\xi}_i} \boldsymbol{m} &= \sum_k \int dV \, \frac{\delta \boldsymbol{A}}{\delta m_k} \partial_{\boldsymbol{\xi}_j} m_k \cdot \partial_{\boldsymbol{\xi}_i} \boldsymbol{m} + \int dV \, \boldsymbol{A} \cdot \partial_{\boldsymbol{\xi}_i \boldsymbol{\xi}_j} \boldsymbol{m} \\
&= \sum_{k,l} \int dV \, \frac{\delta A_l}{\delta m_k} \partial_{\boldsymbol{\xi}_j} m_k \cdot \partial_{\boldsymbol{\xi}_i} m_l + \int dV \, \boldsymbol{A} \cdot \partial_{\boldsymbol{\xi}_i \boldsymbol{\xi}_j} \boldsymbol{m} \\
&= \int dV \boldsymbol{m} \cdot \left(\partial_{\boldsymbol{\xi}_i} \boldsymbol{m} \times \partial_{\boldsymbol{\xi}_j} \boldsymbol{m} \right) + \int dV \, \boldsymbol{A} \cdot \partial_{\boldsymbol{\xi}_i \boldsymbol{\xi}_j} \boldsymbol{m} \\
&= G_{ij}[\boldsymbol{\xi}] + \int dV \, \boldsymbol{A} \cdot \partial_{\boldsymbol{\xi}_i \boldsymbol{\xi}_j} \boldsymbol{m},
\end{aligned}
\tag{2.63}
$$

where in the third line, we used the simmetry properties of the sum in i and j and the definition of the gauge potential for the monopole, see Eq. 2.25. In the total action, the second term will vanish when we consider the term that is proportional to $\boldsymbol{\xi}_i \dot{\boldsymbol{\xi}}_j$. The derivation 2.63 implies that, it is possible to write from the Berry phase, a Poisson bracket of the form

$$
\frac{M_s}{\gamma} \sum_j G_{ij} \{ \boldsymbol{\xi}_i, \boldsymbol{\xi}_j \} = 1.
\tag{2.64}
$$

The damping term γ_i may be obtained in a similar way by using the substitution from Eq. 2.58 into the Rayleigh dissipation term 2.31. From this procedure we obtain the viscosity tensor defined in Eq. 2.60b.

This formalism is valid for any dynamics of the magnetization. In the specific case of topological textures, there is a clear hierarchy on the time scales of the evolution of the dynamical parameters. The stability of these objects allows for the separation between hard modes, corresponding to fast dynamics, and soft modes, corresponding to slow dynamics. [33, 35, 78] Another particularity, is that the soft modes obey the relation 2.64 in pairs. [2, 33, 71] This means that G_{ij} do not depend explicitly on $\boldsymbol{\xi}_i$ and can be inverted. For soft modes, one obtains the following

30

Poisson bracket for the soft modes

$$\{\boldsymbol{\xi}_i, \boldsymbol{\xi}_j\} = \frac{\gamma}{M_s} G_{ij}^{-1}. \tag{2.65}$$

Notice that this Poisson bracket is derived only from the kynectic term of the Lagrangian and does not depend on the specific details of the Hamiltonian. With this Poisson bracket, it is possible to obtain a powerful and rich model independent formalism. [2]

3. DOMAIN WALL CREATION IN FERROMAGNETIC NANOWIRES BY ELECTRIC MEANS

The manipulation of the position and orientation of DWs in ferromagnetic nanowires by electric current is the basis of a proposed new generation of magnetic memory devices. [13, 28, 47, 79, 80] A crucial element for the functionality of these devices is the creation of DWs. Currently, DWs are usually created by applying strong local magnetic fields or perpendicular currents. [13, 81, 82, 83] In the work that was published in PRB, we demonstrated that the creation solely by an applied current along the wire is possible. [1] This presents advantages to respect to the current methods. It allows, for example, for the existence of smaller devices. The theory can also be extended to other configurations. It was shown that the same principle allows for a skyrmion-antiskyrmion pair creation in ferromagnetic thin-films. [84] Within this mechanism, we considered a semi-infinite nanowire with easy axis anisotropy along the wire and a fixed magnetization perpendicular to the easy-axis at the end of the nano-wire, see Fig. 3.1. The fixed magnetization may be due to a strong pinning center or an adjacent permanent ferromagnet. We predicted the existence of a critical current, above which a current is capable of inducing the periodic creation of DWs in this configuration. We were able to also calculate the periodicity of the creation.
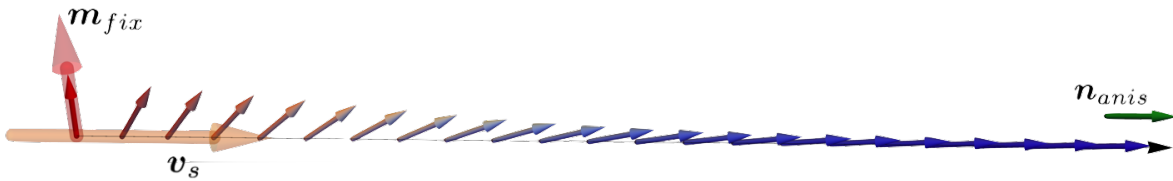
Figure 3.1: Representation of the configuration for DW creation. $\boldsymbol{m}_{fix}$ represent the fixed magnetization, $\boldsymbol{v}_s$ correspond to the applied spin current, and $\boldsymbol{n}_s$ is the direction of the easy-axis.

A major goal of this project was to show that this process is quite general. It does not depend on details of the microscopic properties of the materials and obeys a quite universal law. From

a minimal model, with only exchange and anisotropy interaction, and spin transfer torque, we were able to derive the periodic DW injection. We did not require any "twisting" interactions such as DMI or dipole-dipole interactions. We predicted, however, that if one includes some of these interactions and damping terms it is possible to reduce significantly the critical current.

This chapter is organized as follows: First, we will obtain the existence of the critical current. Given the configuration proposed above, see Fig. 3.1, we shown the existence of different critical currents for the ferromagnetic state and the fixed magnetization. Second, we consider the dynamics of the magnetization for applied currents in the limit just above the critical current. We show that this dynamics can be described in terms of a single parameter, corresponding to the position of a fictitious DW. The dynamics of this parameters reveals a finite period inversely proportional to the square root of the increment of current above the critical current. Finally, we discuss the main results and provide an experimental estimative for the results found in this work.

3.1   Critical current

In this section we derive the existence of critical currents below which the ferromagnetic state and the fixed magnetization configurations are stable. We consider the dynamics given by LLG Eq. 2.7 and the STT contribution for a spin current along the wire, Eq. 2.33,

$$\dot{\boldsymbol{m}} = -\frac{\gamma}{M_s}\boldsymbol{m} \times \frac{\delta\mathcal{H}}{\delta\boldsymbol{m}} - v_s\partial_x\boldsymbol{m} - \beta v_s\boldsymbol{m} \times \partial_x\boldsymbol{m} + \alpha\boldsymbol{m} \times \dot{\boldsymbol{m}}. \tag{3.1}$$

For the effective Hamiltonian $\mathcal{H}$, we consider a minimalist model with only exchange energy and easy-axis anisotropy,

$$\mathcal{H} = a^2 \int dx \left(\frac{J}{2}\left(\partial_x\boldsymbol{m}\right)^2 - \lambda m_x^2\right), \tag{3.2}$$

where a^2 is the area of the cross section of the nanowire. If one substitute the Hamiltonian 3.2 into Eq. 3.1, we obtain

$$\dot{\boldsymbol{m}} = -\frac{\gamma a^2}{M_s}\boldsymbol{m} \times \left(-J\partial_x^2\boldsymbol{m} - 2\lambda\hat{\boldsymbol{e}}_x m_x\right) - v_s\partial_x\boldsymbol{m} + \alpha\boldsymbol{m} \times \dot{\boldsymbol{m}}. \tag{3.3}$$

From this equation[1], one can calculate the critical current for both the ferromagnetic state and the fixed magnetization state. We start by considering the ferromagnetic state. We perform this calculation following the linearization approach from Sec. 2.3.1. The ferromagnetic state $m_f = \pm\hat{e}_x$ satisfies Eq. 3.3, with $\dot{m} = 0$. If we consider perturbations of the ferromagnetic states as spin waves, $m = \hat{e}_x + s$ with $s = s_0 e^{i(wt-kx)}$ and no damping term, we obtain a dispersion relation of the form

$$\omega \propto v_s \pm \sqrt{8\left(\frac{\gamma a^2}{M_s}\right)^2 J\lambda - v_s^2}. \tag{3.4}$$

This means that, for currents $v_s < (\gamma a^2/M_s)\sqrt{8J\lambda}$, the spin waves do not change amplitude, and therefore, will lose energy with the damping process. For spin currents bigger than the value above, the spin waves can increase in amplitude. In this case, the ferromagnetic state is no longer stable under perturbations. Therefore the critical current for the ferromagnetic state is given by $v_s^C = (\gamma a^2/M_s)\sqrt{8J\lambda}$.

The conditions for the stability of the fixed magnetization state can be obtained by analyzing the conserved quantities with $\dot{m} = 0$. To obtain the first quantity, we consider two arguments. First, from the physical point of view, in the presence of damping, $\alpha > 0$, the effective Hamiltonian 3.2 tends to be minimal. This means that we can consider 3.2 as an action that must be minimized. Since it is explicitly independent of x, this implies the conservation of a "Hamiltonian" associated to the "action" 3.2. Second, from a mathematical point of view, if we multiply the Eq. 3.3 by $(m \times \partial_x m)$, we obtain the equation

$$\partial_x\left(\frac{J}{2}(\partial_x m)^2 + \lambda m_x^2\right) = 0. \tag{3.5}$$

It is important to notice that, in the presence of non-adiabatic STT, Eq. 2.35, we need to add to the right hand site a term proportional to $\beta v_s (\partial_x m)^2$.

For the second conserved quantity, we can consider the conservation of magnetic momentum.

---

[1]In this chapter, we will neglect the contribution from the non-adiabatic STT, proportional to the β damping term. Whenever necessary, we will mention the modifications due to this term.

This can be obtained from the x component of Eq. 3.3,

$$\partial_x \left(\frac{\gamma a^2}{M_s} J \hat{\boldsymbol{e}}_x \cdot (\boldsymbol{m} \times \partial_x \boldsymbol{m}) + v_s m_x \right) = 0. \tag{3.6}$$

Tn the presence of non-adiabatic STT, Eq. 2.35, the above equation is proportional to $\beta v_s \hat{\boldsymbol{e}}_x \cdot (\boldsymbol{m} \times \partial_x \boldsymbol{m})$. From the conservation relations 3.5 and 3.6, we can compare their values at infinity, $x \to \infty$, and at the fixed magnetization, $x = 0$, to obtain a critical current given by $v_s^c = (\gamma a^2/M_s)\sqrt{2J\lambda}$, which is half of the critical current for the ferromagnetic state. The idea applied here for nanowires can be extended to thin-films. In this case, a region of fixed magnetization is also responsible for the existence of a critical current above which there is a production of pairs of skyrmions and anti-skyrmions. [84]

For chiral nanowires, we need to introduce DMI. If one introduces Bloch DMI, given by Eq. 2.12a, in a nanowire, we modify the effective Hamiltonian 3.2 and consequently Eq. 3.6,

$$\partial_x \left(\frac{\gamma a^2}{M_s} J \hat{\boldsymbol{e}}_x \cdot (\boldsymbol{m} \times \partial_x \boldsymbol{m}) + \frac{\gamma a^2}{M_s} D m_x^2 + v_s m_x \right) = 0. \tag{3.7}$$

As expected, DMI introduces chirality to the system and increases the angular moment from the DW. Following the previous approach, one find the following relation for the critical current

$$\left| \frac{\gamma a^2}{M_s} D + v_s \right| < v_s^c. \tag{3.8}$$

This relation shows that, with the twisting term due to DMI, different direction of currents have different critical currents.

The above calculations provide a range of spin currents, $v_s^C > v_s > v_s^c$, for which the magnetization dynamics close to the fixed magnetization is not static but the ferromagnetic state is stable. This motivates to study the dynamics in this range of currents. In Refs. [1, 84], it was proven that for currents right above v_{sc} one has the periodic production of topological textures. This is the subject of next chapter.

3.2 DW injection in a nanowire

For currents just above the critical current, the stability of the system allows us to assume that the dynamical behavior won't produce configurations that diverges significantly from the static solutions below the critical current. For this reason, it is interesting to analyze the properties of the static solutions.

From the condition 2.5, one can write $\boldsymbol{m}$ in terms of the functions $\Lambda(x)$ and $\Gamma(x)$ as

$$\partial_x \boldsymbol{m} = (\hat{\boldsymbol{e}}_x \times \boldsymbol{m})\Gamma(x) + [\boldsymbol{m} \times (\hat{\boldsymbol{e}}_x \times \boldsymbol{m})]\Lambda(x), \tag{3.9}$$

with $\partial_x m_x = \Lambda(x)(1 - m_x^2)$. In this basis, Eqs. 3.5 and 3.6 read:

$$\frac{J}{2}(1 - m_x^2)(\Lambda^2 + \Gamma^2) = -\lambda(1 - m_x^2), \tag{3.10}$$

$$\Gamma(1 - m_x^2) = \left(M_s/(\gamma a^2 J)\right) v_s(1 - m_x). \tag{3.11}$$

From the system of equations above, eliminating Γ and using $\partial_x m_x = \Lambda(1 - m_x^2)$ one obtains the following equation

$$(\partial_x m_x)^2 - \left(\frac{M_s}{\gamma a^2 J}\right)^2 \left((v_s^c)^2(1 - m_x^2)^2 - v_s^2(1 - m_x)^2\right) = 0, \tag{3.12}$$

which we can solve by separating variables:

$$x = \frac{\gamma a^2 J}{M_s} \int_0^{m_x} dm_x \left((v_s^c)^2(1 - m_x^2)^2 - v_s^2(1 - m_x)^2\right)^{-1/2}. \tag{3.13}$$

The above integral provides the full DW profile. The boundaries are given by the configuration at the fixed magnetization, where $m_x = 0$ to the magnetization at any other point of the semi-infinite wire. To understand the solution above, it is helpful to visualize the denominator from Eq. 3.13, see Figs. 3.2 and 3.3.

It is relevant to consider an analogy between the magnetization configuration, m_x, along the
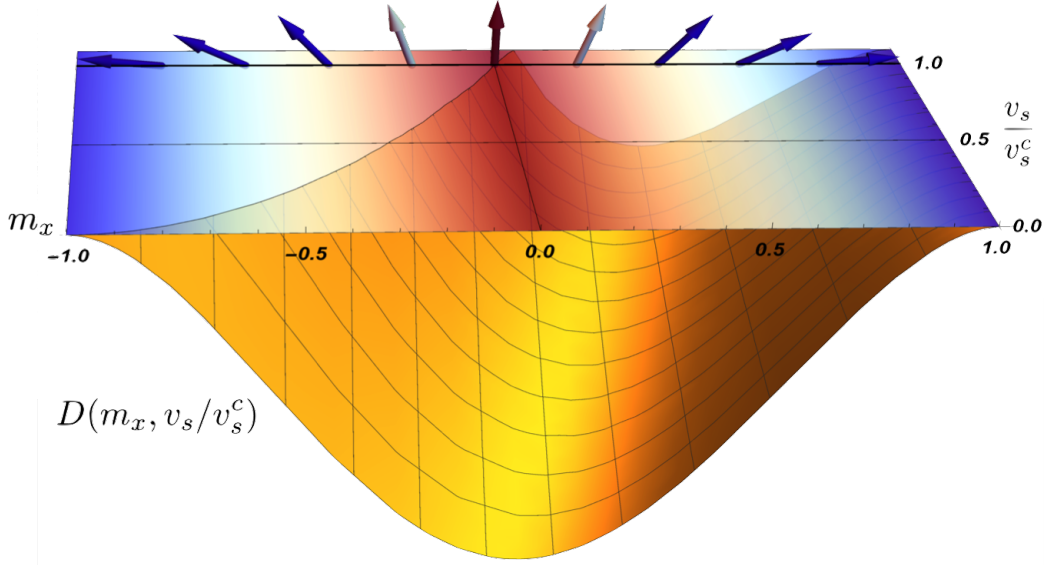
Figure 3.2: Plot of the function $D(m_x, v_s/v_s^c) = -(v_s^c)^2(1-m_x^2)^2 + v_s^2(1-m_x)^2$ of the denominator in terms of the magnetization and the ratio between the current and the critical current. On the horizontal plane, we see the color of the corresponding magnetization, going from blue, in the ferromagnetic state, to red, perpendicular to the ferromagnetic state. Since $-D(m_x, v_s/v_s^c)$ is in a square root, only the negative values provide real solutions to the equation. For $v_s/v_s^c > 1$ there are no solutions that satisfy $m_x = 0$ as we can observe from the plot.

wire,x, as a particle, given by position $\tilde{x}(t)$, with mass $2\left(\gamma a^2 J/M_s\right)^2$ moving in time in a potential well given by $-D(m_x, v_s/v_s^c) - \to -P(\tilde{x}, v_s/v_s^c)$. [1] At infinity, the magnetic moment aligns with the uniaxial anisotropy direction, $m_x(x \to \infty) = 1$, which translates into $\tilde{x}(t \to \infty) = 1$. The magnetization profile, thus, corresponds to a particle that at time zero is at the origin, $\tilde{x}(t = 0) = 0$, and that approaches unity, $\tilde{x}(t \to \infty) = 1$. If one extends the motion to $t < 0$, meaning $x < 0$, we observe an interesting behavior. In this case, since the corresponding energy given by 3.12 is conserved and equal to zero, the full particle motion correspond to an oscillatory motion starting at $t = -\infty$ at $\tilde{x} = 1$ to a point of return $\tilde{x}_0$, defined by $P(\tilde{x}_0, v_s/v_s^c) = 0$, at some time t_0. At the returning point it switches the direction of motion and travels back to $\tilde{x} = 1$. As one can see from Fig. 3.2, the point of return $\tilde{x}_0$ has negative values for $v_s < v_s^c$ so that the particle crosses $\tilde{x} = 0$,
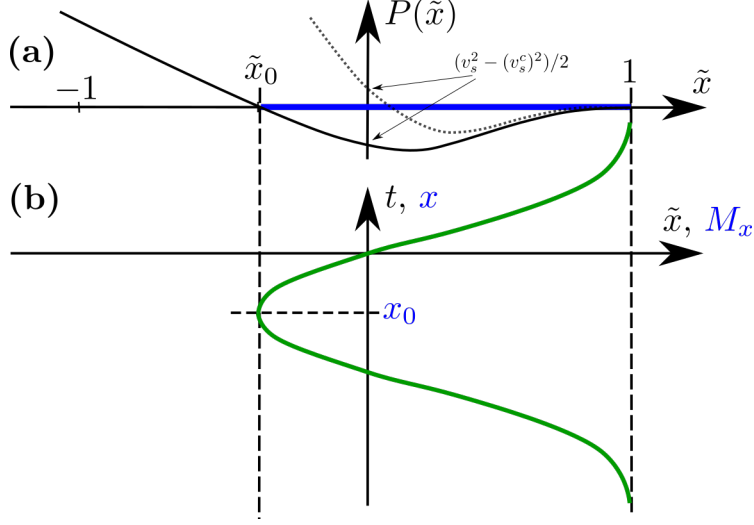
Figure 3.3: Image concerning the definition of x_0 and the magnetization profile. (a) The black line represents the potential $P(\tilde{x})$, which in this thesis stand for $D(m_x, v_s/v_s^c)$ and $\tilde{x} = M_x$, for $v_s < v_s^c$. The allowed interval of the magnetization direction is given by the blue interval. The dotted line shows the same function for $v_s > v_s^c$. (b) Sketch of the magnetization profile, $M_x(x)$. Reprinted from Ref. [1] with permission.

meaning $m_x = 0$, twice. While the second time the particle crosses $\tilde{x} = 0$, correspond to the fixed magnetization, the first time that $\tilde{x} = 0$ correspond to a fictitious DW on the $x < 0$ side of the wire.

The full profile of the magnetization can be characterized, therefore, in terms of the parameter x_0, position of the the magnetization m_x that satisfies $D(m_x, v_s/v_s^c) = 0$. To find the dependence of x_0 in terms of the current, we consider that $(v_s - v_s^c)/v_s^c \ll 1$ and $m_{x0} \lesssim 0$. This allows for the approximation

$$D(m_x, v_s/v_s^c) \approx v_s^c(v_s - v_s^c) - (v_s^c)^2 m_x. \tag{3.14}$$

From this, one finds that the magnetization m_x that is root of $D(m_x, v_s/v_s^c)$ is $m_{x0} = (v_s - v_s^c)/v_s^c$. The position of this magnetization can be found from Eq. 3.13

$$x_0 = \frac{\gamma a^2 J}{M_s} \int_0^{m_{x0}} dm_x \left(v_s^c(v_s - v_s^c) - (v_s^c)^2 m_x \right)^{-1/2}. \tag{3.15}$$

From which we find

$$x_0 = -\frac{\gamma a^2 J \sqrt{2}}{M_s v_s^c} \sqrt{\frac{v_s^c - v_s}{v_s^c}}. \tag{3.16}$$

From the interpretation that x_0 corresponds to a parameter that defines the profile of the magneti-zation configuration for the full wire and allows for, in the case $x_0 < 0$ the existence of a fictitious second DW. One can extrapolate the result to the dynamical case for currents above the critical current. In this case, we incorporate the dynamics of the magnetization profile into the parameter x_0,

$$\boldsymbol{m}(x,t) = \boldsymbol{m}_0 \left(x - x_0(t) \right) + \boldsymbol{s}, \tag{3.17}$$

where $\boldsymbol{m}_0 \left(x - x_0 \right)$ is the static solution with effective spin current $v_{s_{x_0}}$ that solves Eq. 3.16 and $\boldsymbol{s}$ is small and takes into account possible deviations from the proposed solution. Plugging the above ansatz into the LLG Eq. 3.3, one obtains

$$- \dot{\boldsymbol{s}} + \boldsymbol{s} \times \frac{\delta \mathcal{H}}{\delta \boldsymbol{m}_0} + \boldsymbol{m}_0 \times \frac{\delta^2 \mathcal{H}}{\delta \boldsymbol{m}_0^2} \boldsymbol{s} - v_s \partial_x \boldsymbol{s} = \left(v_s - v_{s_{x_0}} - \dot{x}_0 \right) \partial_x \boldsymbol{m}_0. \tag{3.18}$$

A solution of the above equation corresponds to $\boldsymbol{s} \equiv \boldsymbol{0}$, which indicates that our initial assumption is valid if the dynamical parameter obeys the following equation:

$$\dot{x}_0 = v_s - v_{s_{x_0}} = v_s - v_s^c + \frac{M_s^2 (v_s^c)^3}{2\gamma^2 a^4 J^2} x_0^2, \tag{3.19}$$

where we obtained $v_{s_{x_0}}$ from Eq. 3.16. Therefore

$$t = \int dx_0 \left(v_s - v_s^c + \frac{M_s^2 (v_s^c)^3}{2\gamma^2 a^4 J^2} x_0^2 \right)^{-1}. \tag{3.20}$$

Notice that the main contribution comes from $x_0^2 \sim 2\gamma^2 a^4 J^2 (v_s - v_s^c)/[M_s^2 (v_s^c)^3] \to 0$. Outside of this range the integral converges quickly. From this consideration it is justified to calculate the total period T by integrating to infinity, even though the equation above is only valid for small x_0.

The corrections are exponentially small as $(v_s - v_s^c) \to 0$. Finally. we obtain:

$$T = \int_{-\infty}^{\infty} dx_0 \left(v_s - v_s^c + \frac{M_s^2 (v_s^c)^3}{2\gamma^2 a^4 J^2} x_0^2 \right)^{-1} \tag{3.21}$$

$$= \frac{\sqrt{2}\pi\gamma a^2 J}{M_s (v_s^c)^2} \sqrt{\frac{v_s^c}{v_s - v_s^c}}. \tag{3.22}$$

From which we deduce that, for currents just above the critical current, there is a periodic injection of DWs in the nanowire with frequency $f = T^{-1} \sim \sqrt{v_s - v_s^c}$.

3.3 Results

This work was done in collaboration with M. Sitte, K. Everschor-Sitte, T. Vallet, J. Sinova and my advisor A. Abanov, and published on Ref. [1]. The main result was the proof of concept of the injection of DWs in a nanowire by all electrical means given a well defined configuration. Our calculations were based on a minimal model and therefore, is quite general. It does not require any "twisting" term or an assisting magnetic field. The introduction of DMI interactions, that favors the DW formation, reduces the critical current but does not change the production mechanism. We showed the existence of a critical current above which one obtains the periodic creation of DWs. The period is given by a universal exponent, $T \sim (v_s - v_s^c)^{-1/2}$.

For a typical estimative of real values, we consider for example a Permalloy with exchange parameter $J = 1.6 \cdot 10^6 J/m$, and anisotropy strength $\lambda = 10^4 J/m^3$. With these parameters we obtained critical current density of about $4 \cdot 10^8 A/cm^2$.

4. DOMAIN WALL MOTION IN ANTIFERROMAGNETIC AND FERROMAGNETIC NANOWIRES

The low energy dynamics of DWs in ferromagnets can be described in terms of just a pair of soft modes. [33, 35, 85] This description can be extended to certain AFM materials, in which we need two pairs of soft modes. [2] In this work, we proceeded with the analysis from Sec. 2.3.2 and obtained a Hamiltonian formalism for the electrical current and magnetic field driven dynamics of DWs in both FM and AFM case. The effective description is based mostly on the analysis of symmetries and natural scales.

A strength of the Hamiltonian formalism is that it is independent of microscopic details of the material. The complicated nature of the interactions between all the magnetic moments can be simplified to a model for only two dynamical parameters, for which one obtains the interactions based on stability and symmetries properties. This procedure is very powerful and rich as one can study many known aspects of FM and AFM DW dynamics and also include in a natural way various interactions. The formalism provides a well described phase space for the conjugated soft modes within which it is possible to analyze the dynamics for interaction between DWs as well as thermodynamic effects. The concrete results obtained from this work so far were the current and magnetic field driven motion of FM and AFM DWs and a novel orientation switching mechanism by current for AFM DWs. This mechanism can be tested with the recently discovered Néel spin orbit torques and has potential applications to AFM DW based memory devices. We also show that, in the considered structure for the AFM case, it is possible to include within the formalism other effects such as different anisotropies and nanowire inhomogeneity.

This chapter is organized as follows: First, we derive the Hamiltonian formalism for FM DW from the known soft modes, including the dissipation terms. We obtain an effective Hamiltonian in terms of the soft modes and demonstrate how it can be derived solely by symmetry arguments. Second, we extend the formalism to the AFM DW case. We solve certain general cases and propose future experiments.

41

4.1 Domain wall dynamics in ferromagnetic nanowires

A FM DW, as discussed in Sec. 2.2.1, is a stable topological soliton with a natural length scale, given by the DW width Δ, and energy scale, given by the DW energy density $\mathcal{E}_{DW}$. In a nanowire its profile is invariant under a translation of its center, X, and a global rotation around the direction of the ground state. This means that a FM DW is well approximated by a rigid object with particle-like behavior. [86] This approximation is also valid for the current or magnetic field driven low energy excitation motion of the DW, since its profile can not change significantly. The excitations modes related to a change in shape is gapped due to the presence of anisotropy. A similar gap was derived for the ferromagnetic state in Sec. 2.3.1. The dynamics is described then in terms of the two soft modes X, position of the center of the DW, and ϕ, angle of the magnetization at the center of the DW in the plane normal to the ferromagnetic state, see Fig. 4.1.
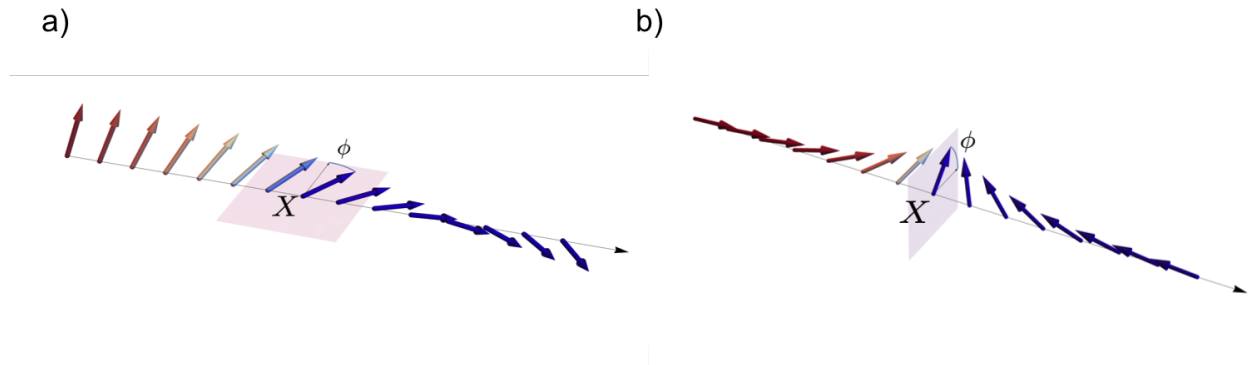
Figure 4.1: Representation of the soft modes in the case of a) ferromagnetic state perpendicular to the wire, and b) ferromagnetic state along the wire, this DW is also called head-to-head DW.

For a rigid DW, a variation of the magnetization m is given in terms of changes variations of the soft modes,

$$dm_i(x) = -dX\partial m_i(x) + d\phi\epsilon_{ijk}n_j m_k(x), \tag{4.1}$$

where $\hat{n}$ is unitary and in the direction of the ferromagnetic state. Substituting this relation into

the definition 2.60a, one obtains that the Poisson bracket in Eq. 2.65 takes the form

$$\{X, \phi\} = \pm 1, \tag{4.2}$$

where the $+$ and $-$ signs depend on the directions at infinity.[1] [2] This means that, as expected, the soft modes x and ϕ are canonically conjugated Hamiltonian variables independent of the microscopic form of the Hamiltonian.

In order to find the total energy, E, for the system, first we notice that the microscopic Hamiltonian $\mathcal{H}$ does not depend explicitly in time. This implies that

$$\dot{E} = \int dx \frac{\delta \mathcal{H}}{\delta m_i(x)} \dot{m}_i. \tag{4.3}$$

If one substitutes the LLG Eq. 3.1 for the nanowire, we notice that the only non-dissipative term is due to the spin current,

$$-v_s \int \frac{\delta \mathcal{H}}{\delta m_i(x)} \partial_s m_i dx = v_s \partial_X E, \tag{4.4}$$

where X is the soft mode corresponding to the DW position. The remaining terms are first order in dissipation α. Since, the characteristic values of the damping term are of the order $\alpha \sim 10^{-3} - 10^{-5}$, we are only interested in terms that are linear in α. From the equation of motion we use that $\epsilon_{ijk} m_j \delta \mathcal{H} / \delta m_k = \dot{m}_i + J \partial m_i$ and obtain

$$\dot{E} - v_s \partial_X E = -\int (\dot{m}_i + v_s \partial m_i)(\alpha \dot{m}_i + \beta v_s \partial m_i) dx. \tag{4.5}$$

For the dissipationless dynamics, $\alpha = \beta = 0$, we obtain the above equation is reduced to $\dot{E} = v_s \partial_X E$. Therefore, the Hamiltonian equations of motion provide the following effective Hamiltonian, $H(X, \phi)$, for the system with applied current,

$$\dot{E} = \{E, H\} = v_s \partial_X E. \tag{4.6}$$

[1]In this chapter, we set the lattice constant to 1 and chose proper dimensions such that $\gamma / M_S = 1$.

The current pumps energy to the system. In the absence of current, the effective Hamiltonian must reduce to the total conserved energy $E(X, \phi)$. From Eq. 4.2 and 4.6 we derive that

$$H(X, \phi) = E(X, \phi) \pm v_s \phi. \tag{4.7}$$

In the Hamiltonian formalism, the above effective Hamiltonian is the only requirement to obtain the effective equations of motion for the FM DW.

The Hamiltonian Eqs. 2.61 for the soft modes X and ϕ take the form

$$\dot{X} = \{X, H\} + \gamma_X, \qquad \dot{\phi} = \{\phi, H\} + \gamma_\phi, \tag{4.8}$$

where the Poisson bracket is given by Eq. 4.2. To calculate the dissipative terms, we expand Eq. 4.5 for the DW motion to the linear order in v_s

$$\begin{aligned}
\dot{E} - v_s \partial_X E = & -\alpha \dot{X}^2 \Delta_X^{-1} + 2\alpha \dot{\phi} \dot{X} \Gamma - \alpha \dot{\phi}^2 \Delta_\phi \\
& + (\alpha + \beta) v_s \dot{X} \Delta_X^{-1} - (\alpha + \beta) \dot{\phi} v_s \Gamma,
\end{aligned} \tag{4.9}$$

where the constants are defined as

$$\Delta_X^{-1} = \int (\partial \vec{m})^2 dx, \quad \Delta_\phi = \int (1 - m_x^2) dx, \text{ and } \quad \Gamma = \int [\vec{e} \times \vec{m}] \partial \vec{m} dx.$$

These parameters depend only on the DW shape. In the absence of chiral interactions, for example, $\Gamma = 0$. [86] From comparing Eq. 4.9 to the expression calculated in 4.8, one obtain the following dissipation terms

$$\gamma_\phi = \mp \alpha \dot{X} \Delta_X^{-1} \pm \beta J \Delta_X^{-1}, \tag{4.10}$$

$$\gamma_X = \pm \alpha \dot{\phi} \Delta_\phi \mp 2\alpha \dot{X} \Gamma \pm (\alpha + \beta) J \Gamma. \tag{4.11}$$

These dissipation terms, the Poisson bracket 4.2 and the Hamiltonian Eqs. 4.8 defines completely

the current driven dynamics of FM DWs up to linear terms in α and β. From this powerful formalism, it is possible to reproduce with ease several aspects of FM DW dynamics described in the literature. [35, 86]

4.2 Domain wall motion in an antiferromagnetic nanowires

We extend the Hamiltonian formalism of FM DW dynamics to include AFM DWs. Diverse studies, both theoretical and experimental, of the AFM dynamics have received great attention due to new experimental methods to detect, create and manipulate magnetic configurations in these systems. [57, 56, 87, 88, 89, 90, 91, 92, 93, 94, 95, 96] In Ref. [2] we addressed an important problem of obtaining an efficient description of the current and magnetic field driven dynamics of AFM DWs.
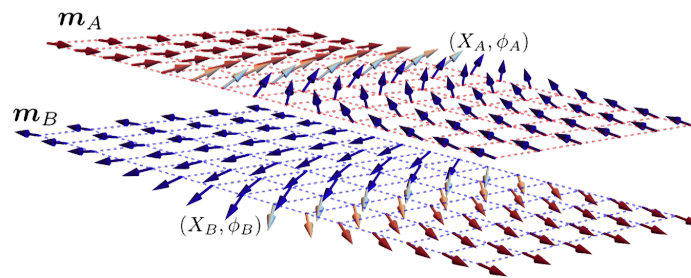
Figure 4.2: A sketch of antiferromagnetic domain wall as a composite of two FM DW in the sublattices. Each FM DW is described by its own set of soft modes. One FM DW is head-to-head (A) and the other is tail-to-tail (B).

For the description of a typical quasi-one-dimensional AFM nanowire, we considered the separation into two sub lattices according to Sec. 2.1.4. We assume that each electron lives on its own sublattice and interacts only with the magnetization of the same sublattice. In the presence of AFM

DW, the separation between different sublattices is not perfect. We assume, however, that the DW width is much larger than the electronic coherence length. Thus, the corrections to this picture are expected to be small. Even though, the potential difference in each sublattice may be the same, it is not necessary that the current is the same, due to possible different resistivities in each sublattice. To simplify the picture, we will assume that given the scales considered, the currents along both sublattices is the same.

To satisfy the AFM DW picture, we need to consider that, each ferromagnetic sublattice contains a FM DW. They are, however, at opposite orientations. For example, if one is head-to-head, the other is tail-to-tail, see Fig. 4.2. In this picture, the dynamics for the DWs on each sublattice is described by the pair of soft modes (X_A, ϕ_A) and (X_B, ϕ_B). The center of the AFM DW is given by $X = \frac{1}{2}(X_A + X_B)$, while $X_A - X_B$ gives the total magnetization of the AFM DW along the nanowire. Analogously, $\phi_B - \phi_A$ is the angle between the directions of the local magnetic moments at the center of the DWs. To simplify the model considered, we also assume that the DW parameters Δ_ϕ, Δ_X, α, and β are the same for the two DWs, and that the DWs are planar, i.e. $\Gamma = 0$.

From the above assumptions, we can write an effective Hamiltonian for the whole system given by $H(X_A, \phi_A, X_B, \phi_B)$. Given the Hamiltonian equations 4.8 and the Poisson bracket 4.2 for each sublattice, with the remark that one is tail-to-tail and the other one head-to-head, we obtain the following equations of motion:

$$\dot{X}_{A,B} = \{X_{A,B}, H\} \mp \alpha \dot{\phi}_{A,B} \Delta_\phi, \tag{4.12a}$$

$$\dot{\phi}_{A,B} = \{\phi_{A,B}, H\} \pm \frac{\alpha}{\Delta_X} \dot{X}_{A,B} \mp \frac{\beta}{\Delta_X} v_{s\,A,B}, \tag{4.12b}$$

where upper and lower signs are for sublattices A and B, respectively. From general assumptions, we can deduce the effective Hamiltonian H. Due to the opposite direction of the magnetizations in the sublattices, we obtain that due to the interaction with spin current and an external magnetic

field h, we obtain

$$H(X_A, \phi_A, X_B, \phi_B) = E(X_A, \phi_A, X_B, \phi_B) - hX_A + hX_B - v_{sA}\phi_A + v_{sB}\phi_B, \qquad (4.13)$$

where $E(X_A, \phi_A, X_B, \phi_B)$ contains the coupling between the DWs and the individual energy for each sublattice. In a translationally invariant nanowire, the coupling must be independent of $X_A + X_B$. The picture changes if there are impurities or geometrical constraints. In the case of a hourglass nanowire, for example, we can assume an expansion of the potential and add a term $\Omega(X_A^2 + X_B^2)/2$ to the energy E, where Ω is a constant inversely proportional to the nanowire curvature. [80]

From the antiferromagnetic exchange tendency to minimize the absolute value of the magnetization vector $\boldsymbol{M} = \boldsymbol{m}_A + \boldsymbol{m}_B$, we can deduce the coupling between the DWs. The minimum energy of the coupling is reached at $X_A - X_B = 0$ and $\phi_A - \phi_B = \pi$. Expanding for small $|X_A - X_B|$ and the first harmonic of the angular dependence, we find

$$E(X_A, \phi_A, X_B, \phi_B) = \frac{\Delta_1}{2}(X_A - X_B)^2 + \Delta_2 \cos(\phi_A - \phi_B), \qquad (4.14)$$

where the constants Δ_1 and Δ_2 are of the order of $J_{AF}\Delta_X^{-2}$ and J_{AF}, respectively, and J_{AF} is the antiferromagnetic exchange constant. To introduce easy-axis anisotropy, it is required to add the corresponding effective term $-\lambda\left(m_{Az}^2 + m_{Bz}^2\right)$ to the energy.

With the effective Hamiltonian given by Eqs. 4.13 and 4.14, the Hamiltonian Eqs. 4.12 become

$$\dot{X}_{A,B} = \Delta_2 \sin(\phi_A - \phi_B) \mp \alpha \dot{\phi}_{A,B}\Delta_\phi + v_s, \qquad (4.15a)$$

$$\dot{\phi}_{A,B} = \Delta_1(X_A - X_B) - h \pm \frac{\alpha}{\Delta_X}\dot{X}_{A,B} \mp \frac{\beta}{\Delta_X}v_s, \qquad (4.15b)$$

where we assumed that the easy-axis magnetic anisotropy and the applied magnetic field h are along the wire. The formalism, however, can incorporate different directions, given a suitable

change of notations. The equations of motion 4.15a and 4.15b are one of the main results of this chapter. They provide a comprehensive description of the current and field driven dynamics of AFM DW.

For a better understanding of the influence of each interaction, we will first analyze the current and magnetic field driven dynamics independently. For the current induced motion of AFM configurations, many aspects are well known. [97, 98, 99] These results may be obtained naturally from the described Hamiltonian formalism. Setting $h = 0$ and from a proper combination of the Eqs. 4.15a and 4.15b we obtain

$$\dot{X}_A - \dot{X}_B = -\alpha(\dot{\phi}_A + \dot{\phi}_B)\Delta_\phi, \tag{4.16}$$

$$\dot{\phi}_A + \dot{\phi}_A = 2\Delta_1(X_A - X_B) + \frac{\alpha}{\Delta_X}(\dot{X}_A - \dot{X}_B). \tag{4.17}$$

One can solve this system up to first order in dissipation to obtain

$$\dot{X}_A - \dot{X}_B = -2\alpha\Delta_\phi\Delta_1(X_A - X_B). \tag{4.18}$$

Which corresponds to an exponentially decaying solution for $X_A - X_B$ and indicates that it evolves to the steady state $X_A = X_B$. Also from Eqs. 4.15a and 4.15b, one obtains

$$\dot{\phi}_A - \dot{\phi}_B = \frac{2\alpha}{\Delta_X}\dot{X} - \frac{2\beta}{\Delta_X}v_s, \tag{4.19a}$$

$$\dot{X} = \Delta_2\sin(\phi_A - \phi_B) - \alpha\Delta_\phi\frac{\dot{\phi}_A - \dot{\phi}_B}{2} + v_s, \tag{4.19b}$$

where $X = (X_A + X_B)/2$ corresponds to the position of the AFM DW. Similarly to the previous system, by solving up to first order in dissipation, we obtain

$$\dot{X} = \Delta_2\sin(\phi_A - \phi_B) + v_s. \tag{4.20}$$

The above set of equations gives the that the dynamics of AFM DW under the influence of an

electrical current moves with constant velocity v and relative angle $\phi_A - \phi_B$ given by

$$v = \frac{\beta}{\alpha} v_s, \qquad \sin(\phi_A - \phi_B) = -\frac{v_s}{\Delta_2}(1 - \beta/\alpha). \qquad (4.21)$$

There is no relative rotation between the DWs in the sublattices, i.e. $\dot{\phi}_A - \dot{\phi}_B = 0$. In this translational motion, there is a total magnetic moment perpendicular to the nanowire for the AFM DW given by $\Delta_X v_s / v_s^c$, where $v_s^c = \frac{\alpha \Delta_2}{|\alpha - \beta|}$ is a critical current up to which the above solution solution exists. This result was first reported for the case of FM DWs and motivated the mechanism of DW creation in FM nanowires. [1, 86, 100] This current is generally large, since Δ_2 is of the order of the exchange constant. Physically this critical current corresponds to the situation when the magnetizations on the two sublattices rotate with respect to each other and eventually point in the same direction due to damping. For currents above the critical current, the total magnetic moment perpendicular to the nanowire oscillates in time with period $T = \frac{\Delta_X}{2\alpha\Delta_2} \frac{2\pi}{\sqrt{(v_s/v_s^c)^2 - 1}}$. The velocity of the AFM DW will not be constant as well, with an average velocity given by $\bar{v} = \frac{\beta v_s}{\alpha} - \frac{v_s \Delta_2}{v_s^c}\left(1 - \sqrt{(v_s/v_s^c)^2 - 1}\right)$.

The dynamics of the AFM DW changes for different angles of the applied magnetic field. First we consider a magnetic field perpendicular to the nanowire. In this case, the magnetic field does not couple with the angles of the DWs according to the Zeeman interaction, $-h(\sin\phi_A + \sin\phi_B)$, where h is the product between the magnetic field amplitude and the magnetic moment of the DW. Such term does not change the equations of motion for $\dot{\phi}_A$ and $\dot{\phi}_B$, see Eqs. 4.15a and 4.15b. It modifies the equations for $\dot{X}_{A,B}$ by a term $\pm h \cos \phi_{A,B}$. From Eqs. 4.12, we obtain

$$\dot{X}_{A,B} = \Delta_2 \sin(\phi_A - \phi_B) \mp \alpha \dot{\phi}_{A,B} \Delta_\phi + v_s \pm h \cos \phi_{A,B}, \qquad (4.22a)$$

$$\dot{\phi}_{A,B} = \Delta_1(X_A - X_B) \pm \frac{\alpha}{\Delta_X} \dot{X}_{A,B} \mp \frac{\beta}{\Delta_X} v_s. \qquad (4.22b)$$

A simple solution for the steady state at small current, v_s, and magnetic field, h, is given by $X_A = X_B = X$ and $\dot{X} = \frac{\beta}{\alpha} v_s$. This translational motion is equivalent to the one obtained by pure

current driven motion. For the angles, however, we obtain $\phi_A = \pi + \phi_B$ and

$$\cos \phi_A = -\frac{v_s}{h}(1 - \beta/\alpha). \tag{4.23}$$

From Eqs. 4.22a and 4.22b, we observe the possibility of an angle switching mechanism by switching the the current with constant applied magnetic field. Due to different observable properties of different orientations in a AFM DW, this mechanism is relevant for possible applications to memory devices and deserves further analysis.

It is important to notice that a weak magnetic field applied parallel to the nanowire induces a precession of the AFM DW. This precession is extremely slow with period inversely proportional to the small applied magnetic field. We search, therefore, for a fast mechanism that combines the use of a time dependent current along the nanowire and an applied perpendicular magnetic field.

Given an initial configuration for which $X_A = X_B = X$ and $\phi_A = \pi - \phi_B = \phi$, it is possible to find several solutions for a time dependent current that associated to the equations of motion (4.22a) and (4.22b) produces a flip of the orientation of the domain wall, $\phi_{A,B} \to \phi_{B,A}$. A solution of this current may be found analytically, up to linear terms in dispersion, for a defined ϕ evolution is given by

$$v_s(t) = \frac{1}{\alpha - \beta}\left(\Delta_X \dot{\phi} + \alpha \cos \phi \left(2\Delta_2 \sin \phi - h\right)\right), \tag{4.24}$$

where $\dot{\phi}$ depends on the desired movement of the DW angle. Many possible paths that allows the switch may be conceived. For the path that minimizes the Ohmic losses and with finite time of switching given by T, we find that the evolution of ϕ must follows the following equation

$$t = \frac{\Delta_X}{\gamma} \int_{\phi_0}^{\phi(t)} \frac{d\phi}{\sqrt{\frac{E_T}{\gamma^2} + \cos^2 \phi \left(\sin \phi - \sin \phi_0\right)^2}}, \tag{4.25}$$

where $\gamma = 2\Delta_2\alpha$ and $E_T = \Delta_X^2 \dot{\phi}_0^2$ is the constant related to the time of switching T by

$$T = \frac{\Delta_X}{\gamma} \int_{\phi_0}^{\pi - \phi_0} \frac{d\phi}{\sqrt{\frac{E_T}{\gamma^2} + \cos^2 \phi \left(\sin \phi - \sin \phi_0\right)^2}}. \tag{4.26}$$

and $\sin \phi_0 = \frac{h}{2\Delta_2}$ corresponds to the initial state. The time of switching, T, is about h^2 times faster than the precession by a magnetic field parallel to the wire. For the measurement of the switch one can consider the works in Refs. [101]. Moreover, the switching process is associated to a time dependent total magnetic moment, see Fig. 4.3 which can also be measured experimentally and allows for an indirect measure of the process.
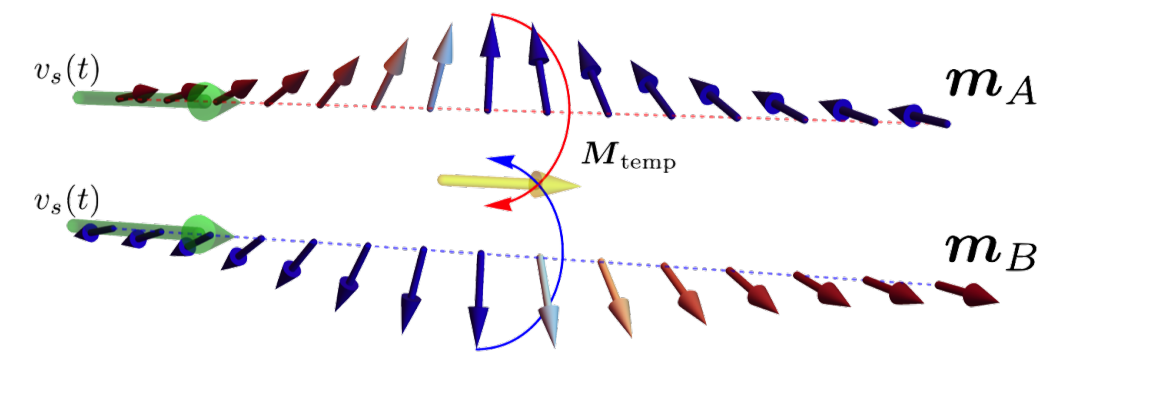
Figure 4.3: A sketch of the switching mechanism. We consider the two A, B sublattices with same applied time dependent current $v_s(t)$. As the DWs flip directions, there is the appearance of a total magnetization M_{temp} in the same direction as the applied magnetic field.

In the present formulation the direction of the magnetic field in the plane perpendicular to the nanowire is arbitrary. This is due to the rotation symmetry of the easy axis anisotropy. This mechanism, however, can be optimized in the presence of transverse anisotropy. In this case, the current required for the switching is influenced both by the magnitude of the current and the magnetic field, as well as its orientation compared to the transverse anisotropy.

5. EFFECTIVE STRING DESCRIPTION OF A DOMAIN WALL IN A FERROMAGNETIC THIN FILM

Experiments in thin films, see Refs. [27, 102, 103, 104, 105], reveal rich configurations for DWs including curved DWs and vortex DWs, [106], which can not be captured in the one-dimensional description of Sec. 4. In thin films, there are two dimensions with dimensions bigger than the DW width, Δ. For this reason, it is possible to observe new dynamics along the DWs, which assumes a string like profile. For three dimensional materials in the absence of chiral interactions, it was proposed by Slonczewski in 1972 a description in terms of smooth surfaces. [85] It was not considered, however, bigger curvatures. These curvatures becomes extremely relevant in the case of chiral materials. In these systems, there is another relevant topological objects, skyrmions, which are stabilized by the chiral interactions. By including curvatures in DWs, it is possible to also describe skyrmions. In order to obtain the dynamics of the extra degrees of freedom, we extend the formalism of the previous section and describe DWs in thin films as strings.

This chapter is organized as follows: First, we present the effective description of a DW as a string. We provide the ansatz for the DW magnetization profile as an extended object and obtain the associated total energy. We also discuss how to include skyrmions within the description of curved DWs. Second, we obtain the effective action that describes the dynamics in terms of the new dynamical parameters. Finally, we consider closed DWs and obtain the excitation modes for large skyrmions.

5.1 String domain wall description

Even though the arguments are model independent, based on scaling factors and symmetries of the system, for a concrete approach we will consider a chiral ferromagnetic film with thickness τ, much smaller than the DW width, and easy axis anisotropy normal to the surface. [40, 107, 108]

The micromagnetic Hamiltonian for such object is given by

$$\mathcal{H} = \tau \int d^2x \left(\frac{J}{2} |\nabla \hat{\boldsymbol{m}}|^2 + \lambda(1 - m_z^2) \right.$$

$$\left. + D \left(m_z \nabla \cdot \boldsymbol{m}_\perp - \boldsymbol{m}_\perp \cdot \nabla m_z \right) \right), \tag{5.1}$$

where $\boldsymbol{m}_\perp$ is the vector of the in-plane components of the magnetization m_x, m_y. For $D \geq 4\sqrt{J\lambda}/\pi$ the ground state is given by a helix, [59] which can be viewed as a periodic structure of DWs. In order to describe single DWs, we consider $D < 4\sqrt{J\lambda}/\pi$. The contribution of the dipole-dipole interaction is incorporated as a correction to the out-of-plane anisotropy, see Eq. 2.16.
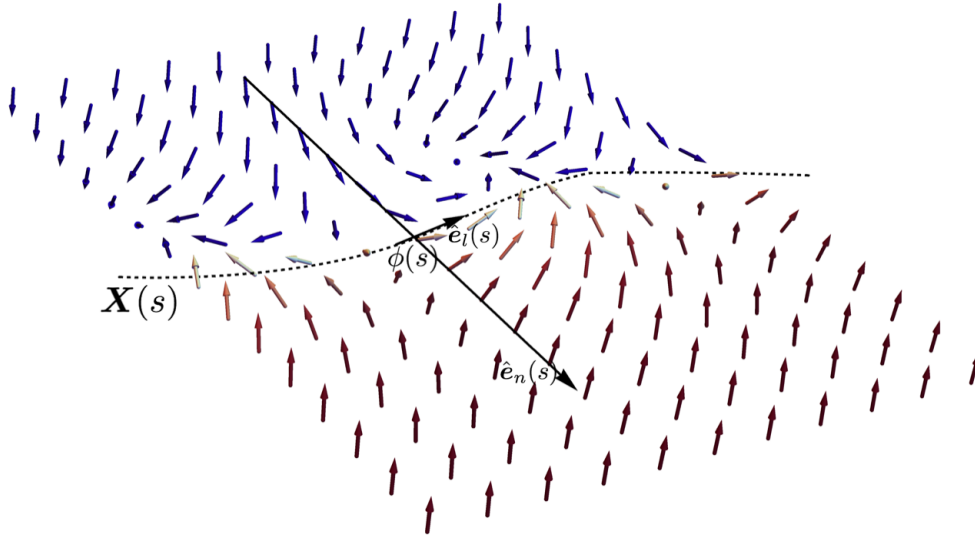
Figure 5.1: A sketch of a DW string. The curve is given by $\boldsymbol{X}(s)$. We define a basis given by the longitudinal vector, $\hat{e}_l$, and a normal vector, $\hat{e}_n$. The magnetization profile along the normal direction corresponds to a rigid one-dimensional DW. The angle between the magnetization along the curve and the normal direction correspond to the field $\Phi(s)$.

In this material, we consider an extended DW as a curve $\boldsymbol{X}$, along which the magnetization is

in plane,

$$\boldsymbol{X}(s) = (x(s), y(s), 0), \tag{5.2}$$

where s is a parameter along the curve. We define a local basis given by the unitary longitudinal vector $\hat{\boldsymbol{e}}_l(s)$ and the unitary normal vector $\hat{\boldsymbol{e}}_n(s)$

$$\hat{\boldsymbol{e}}_l = \frac{\boldsymbol{X}'}{|\boldsymbol{X}'|}, \quad \hat{\boldsymbol{e}}_n = \hat{\boldsymbol{e}}_l \times \hat{\boldsymbol{e}}_z, \tag{5.3}$$

where for any function $f(s)$ we define $f' \equiv \partial_s f$ and $|\boldsymbol{X}'| = \sqrt{(\partial_s x)^2 + (\partial_s y)^2}$. Note that $\hat{\boldsymbol{e}}'_l = k\hat{\boldsymbol{e}}_n$, where the function $k \equiv k(s)$ is related to the local curvature $\kappa(s)$ via $k = |\boldsymbol{X}'|\kappa$. From this assumption, there is a transformation from the Cartesian basis $\hat{\boldsymbol{e}}_x, \hat{\boldsymbol{e}}_y$ into the basis $\hat{\boldsymbol{e}}_n, \hat{\boldsymbol{e}}_l$ along the curve,

$$x, y \rightarrow n, l, \tag{5.4}$$

where n, l are the coordinates along the vectors $\hat{\boldsymbol{e}}_n, \hat{\boldsymbol{e}}_l$, respectively,

$$n(s) = (\boldsymbol{x} - \boldsymbol{X}(s)) \cdot \hat{\boldsymbol{e}}_n(s), \quad l(s) = (\boldsymbol{x} - \boldsymbol{X}(s)) \cdot \hat{\boldsymbol{e}}_l(s). \tag{5.5}$$

Here $\boldsymbol{x}$ denotes any position in space and the parameter l takes values between zero and the length of the extended DW. The relation between the parameters s and l are given by

$$dl = ds|\boldsymbol{X}'|, \tag{5.6}$$

and the curvature κ is defined as

$$\partial_l \hat{\boldsymbol{e}}_l \equiv \kappa \hat{\boldsymbol{e}}_n = \frac{k}{|\boldsymbol{X}'|}\hat{\boldsymbol{e}}_n, \tag{5.7}$$

where in the last equality we have used Eq. 5.6.

We assume that, in the normal direction to the DW, the magnetization profile is fully described by a rigid one-dimensional DW. Since we can associate to such DWs the soft modes X, ϕ, we
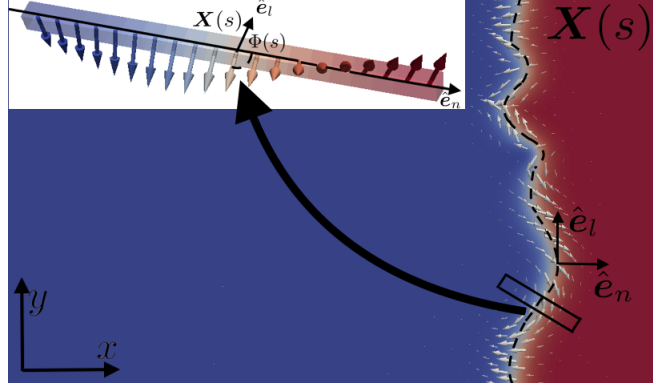
Figure 5.2: Image concerning the ansatz for the DW string. It is a sketch of a smoothly curved DW string given by the curve $\boldsymbol{X}(s)$. We assume that everywhere along the curve, the radius of curvature is much bigger than the DW width, Δ. We define a basis given by the longitudinal vector, $\hat{\boldsymbol{e}}_l$, and a normal vector, $\hat{\boldsymbol{e}}_n$. On the top left corner, we show a typical cross section along the curve with the representations of $\boldsymbol{X}(s)$ and $\Phi(s)$ for each cross section. Reprinted from Ref. [3] with permission.

generalize the soft mode description to $\boldsymbol{X}(s)$, $\Phi(s)$ as functions along the curve. The magnetization field, $\boldsymbol{m}$ close to the DW is given by

$$\hat{\boldsymbol{m}} = \cos \Phi(l) \sin \theta(n) \hat{\boldsymbol{e}}_n(l) + \sin \Phi(l) \sin \theta(n) \hat{\boldsymbol{e}}_l(l)$$
$$+ \cos \theta(n) \hat{\boldsymbol{e}}_z, \tag{5.8}$$

where $\theta(n(s))$ corresponds to a rigid DW centered at position $\boldsymbol{X}(s)$, see Fig. 5.1 and 5.2.

For thin films without periodic boundary conditions, one needs to consider the influence of the boundaries into the DW profile. The DMI and dipole-dipole interactions impose extra conditions close to the edges. In general, one can consider these conditions as perturbations to the bulk state. The bulk state can be obtained from considering periodic boundary condition.

In this work we will neglect possible perturbations due to boundary conditions by considering only periodic boundary conditions or closed DWs. The effective energy obtained from the Hamiltonian 5.1 with periodic boundary conditions in terms of the effective coordinates is given

by

$$\mathcal{H}_{\text{eff}} = \tau \int ds \Big(c_{\mathcal{E}} \mathcal{E} |\boldsymbol{X}'| + \frac{c_{\kappa} J}{|\boldsymbol{X}'|} (\Phi' - k)^2 $$
$$+ D \left(\pi |\boldsymbol{X}'| - c_d k \right) \cos \Phi \Big), \tag{5.9}$$

where $c_{\mathcal{E}}$, c_{κ} and c_d are dimensionless constants that depend on the exact profile of the DW along the normal direction $\hat{e}_n$. For systems in which the domain wall profile is point symmetric to respect to the center of the domain wall, we have that $c_d = 0$. An important feature of the effective Hamiltonian above is that it is invariant under reparametrization. The first term in Eq. 5.9 is proportional to the length of the DW and is minimized by a straight line. The second term describes the fact that bending the DW leads to a changes in Φ' and vice versa. In the absence of DMI the energy is invariant under global rotations of the azimuthal angle of the DW. [5] The picture changes as we include a chiral interaction. Since it breaks inversion symmetry, it directly couples the azimuthal angle Φ with the curvature and the length of the DW curve. This feature, not considered in previous works, makes the the dynamics of the extended DW more complex.

Within the above formalism, the Zeeman interaction due to an external magnetic field can also be incorporated. In this case, the boundary condition will depend also on the relative positions of the string ends. [109, 110]

As an application of the string DW configuration as specified in Eq. 5.8, we can calculate the topological charge, see Eq. 2.44, associated to the string,

$$Q = \frac{1}{2\pi} \int ds \, (k - \Phi'). \tag{5.10}$$

For periodic boundary conditions, this charge must be conserved in the continuum approximation and the integrals over Φ' and k are quantized. The conservation is not required in the case for open boundary conditions. [111, 112]

As we consider closed DWs, the contribution to the Eq. 5.10 from the integral over k is ± 1.

Thus, it is possible to describe smoothly deformed skyrmions, in the limit of big average radius, $R \gg \Delta$, as closed DWs, see Fig. 5.3. Other bounded magnetic configurations, including worm domains and magnetic droplets, may be derived from different functions of Φ that satisfies the corresponding topological charge. The solution for a closed DW that minimizes the Hamiltonian 5.1 is given by a circular skyrmion with radius $R = \Delta \sqrt{c_{\mathcal{E}}/(c_\kappa - \pi D/\mathcal{E})}$ and a constant azimuthal angle $\Phi = \pi$ along the curve. [59] For the radially symmetric case, the soft mode description reduces to two globally defined soft modes, $\{R, \Phi\}$, the radius of the skyrmion and the azimuthal angle of the in-plane magnetization along the radius. [74]
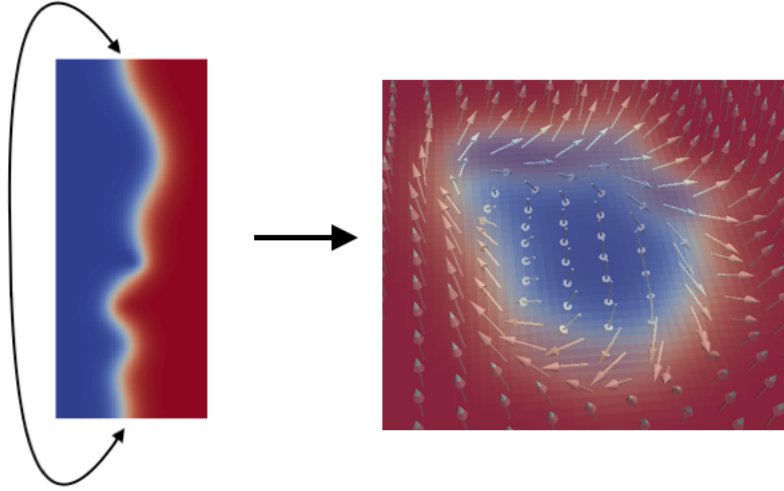
Figure 5.3: Image concerning the skyrmion as a closed DW string. In this figure, we present a sketch between the relation of a skyrmion and a DW string with periodic boundary conditions. Reprinted from Ref. [3] with permission.

5.2   Effective dynamics of DW strings

In order to obtain the time evolution of a DW string configuration, it is necessary to obtain an effective description from the LLG equation. First, following the approach from Sec. 2.3.2, we derived an effective Action for the DW string for the energy conserving dynamics. Given the effective Hamiltonian 5.9, it is also necessary to calculate the spin Berry phase 2.28 in terms of the soft mode fields $\boldsymbol{X}(s)$ and $\phi(s)$. From substituting the DW string ansatz 5.8 into Eq. 2.28, we

obtain

$$S_B = -\tau c_\gamma \int dt \int ds |\boldsymbol{X}'| (\dot{\boldsymbol{X}} \cdot \hat{\boldsymbol{e}}_n) \left(\Phi - \arccos\left(\hat{\boldsymbol{e}}_n \cdot \hat{\boldsymbol{e}}_x \right) \right), \qquad (5.11)$$

where $c_\gamma = 2M_s/\gamma$. For a better understanding of this formula, we consider a special case where Φ is globally defined, i.e. $\Phi' = 0$. In this case, the Berry phase 5.11 simplifies to

$$S_B = -\tau c_\gamma \int dt \, \Phi \dot{A} + \tau c_\gamma \int dt \int ds |\boldsymbol{X}'| (\dot{\boldsymbol{X}} \cdot \hat{\boldsymbol{e}}_n) \arccos\left(\hat{\boldsymbol{e}}_n \cdot \hat{\boldsymbol{e}}_x \right), \qquad (5.12)$$

where by A we define the area of the ferromagnetic domain with $m_z = -1$. The first term reveals that A and Φ are conjugated soft modes. This is equivalent to a nanowire, where the area A is given by the position of the DW. [2] The corresponding Poisson bracket is $\{\Phi, A\} = 1/(\tau c_\gamma)$. An important remark is that, since an external out-of-plane magnetic field couples directly to A, it produces, as expected, a precession of the angle Φ. The second term is related to the chirality of the magnetic moment. In the presence of a magnetic field, a magnetic moment precesses with a well defined direction.

Given the effective Berry phase 5.11 and the effective Hamiltonian 5.9, one obtains the full effective action 2.29 that describes the undamped motion of the magnetic texture. The undamped effective LLG equation for the soft modes fields follows from the variational principle.

For the damped dynamics, it is necessary to also calculate the corresponding effective Rayleigh dissipation functional 2.31. If we plug in the ansatz of the DW string 5.8 into Eq. 2.31, we obtain

$$\mathcal{R}[\dot{\hat{\boldsymbol{m}}}] = \frac{\alpha \tau M_s}{2\gamma} \int dl \left(c_\Phi (\dot{\Phi} + \frac{d}{dt} \left(\arccos\left(\hat{\boldsymbol{e}}_n \cdot \hat{\boldsymbol{e}}_x \right) \right))^2 + c_X \left(\dot{\boldsymbol{X}} \cdot \hat{\boldsymbol{e}}_n \right)^2 \right). \qquad (5.13)$$

The constants c_Φ, c_X are positive and dimensionless and arise from the integration along the $\hat{\boldsymbol{e}}_n$ direction, along which the rigid profile is well defined. They depend only on the specific shape of the profile.

With Eqs. 5.11, 5.9 and 5.13, the variational principal 2.23 gives the full dynamics for the string DW, according to the LLG equation and the micromagnetic model. For concrete results, we apply

58

the effective model to a specific case of large skyrmions.

5.3 Effective dynamics of Skyrmions as closed DW strings

For the magnetic skyrmion configuration as a closed DW string we assume the following curve

$$\boldsymbol{X}(s,t) = r(s,t)(\cos(s), \sin(s), 0), \tag{5.14}$$

where $s = [0, 2\pi)$, and $r(s)$ is a smooth function with $r(0,t) = r(2\pi, t)$. Such an ansatz includes circular and smoothly deformed magnetic skyrmions. For a curve given by Eq. (5.14), the effective spin Berry phase is

$$S_B = -\tau c_\gamma \int dt \int_0^{2\pi} ds \left(\Phi - \arctan \left(\frac{r'}{r} \right) \right) r\dot{r}. \tag{5.15}$$

The term depending on $\arctan(r'/r)$ is associated to the chiral properties of the skyrmion. For the soft modes corresponding to the position of the skyrmion, it provides the Poisson bracket associated to the gyrotropic motion and the Magnus force. [34] In general, considering higher order excitation modes, this term is associated to different speeds of propagation for waves in clockwise and counterclockwise motion.[74] The undamped equations of motion for the local radial distance r and the azimuthal angle Φ of the closed DW are

$$c_\gamma r\dot{r} = \left(\frac{2Jc_\kappa}{|\boldsymbol{X}'|} (\Phi' - k) \right)' + D \sin \Phi \left(\pi |\boldsymbol{X}'| - c_d k \right), \tag{5.16a}$$

$$-\tau c_\gamma \dot{\Phi} = \frac{1}{r} \frac{\delta}{\delta r} \left(\mathcal{H}_{\text{eff}} - \tau c_\gamma r\dot{r} \arctan \left(\frac{r'}{r} \right) \right), \tag{5.16b}$$

where $|\boldsymbol{X}'| = \sqrt{r^2 + r'^2}$ and $k = (\arctan(r'/r))' - 1$. These equations allows us to understand the dynamics of skyrmions in the limit of large radius. First we notice that, if one integrates Eq. 5.16a along the whole curve, one obtains the dynamics for the total area of the skyrmion,

$$\dot{A} = \frac{\pi D}{c_\gamma} \sin \Phi \left(2c_d + \int_0^{2\pi} ds |\boldsymbol{X}'| \right). \tag{5.17}$$

It is important to notice that the area of the skyrmion must be conserved in the absence of DMI. Another property obtained from the absence of DMI is that Eq. (5.16a) has the form of a continuity equation, i.e. $\dot{\rho} = \partial_s j$. The density ρ is given by the area per unit length and the current j corresponds to the density of topological charge per local infinitesimal length. The existence of Bloch lines, which corresponds to a concentration of topological charge, therefore, can generate strong deformations of the DW.

For small deformations, r, of the circular skyrmion with radius R_0, $R_0 \gg r$, and point-symmetric DWs, $c_d = 0$, Eqs. 5.16a and 5.16b provides in a natural way the excitation modes of skyrmions. In this limit we obtain the following equations for r and Φ,

$$c_\gamma \dot{r} + \frac{2c_\kappa}{R_0^3} \left(\partial_s r + \partial_s^3 r \right) = -c_\kappa \left(1 - \frac{1}{2R_0^2} \right) \Phi + c_\kappa \frac{\partial_s^2 \Phi}{R_0^2}, \tag{5.18a}$$

$$R_0 \left(c_\gamma \dot{\Phi} + \frac{2c_\kappa}{R_0^3} \left(\partial_s \Phi + \partial_s^3 \Phi \right) \right) = 2c_\gamma \partial_s \dot{r} + \frac{c_\kappa}{R_0^3} \left(r + 2\partial_s^2 r + \partial_s^4 r \right), . \tag{5.18b}$$

where we used that $R_0 = \Delta \sqrt{c_\mathcal{E} / (c_\kappa - \pi D / \mathcal{E})}$. We also renormalized the paratemeters such that r and R_0 are divided by DW width Δ, and are dimensionless, and c_κ is divided by J. These equations have non-trivial solutions $\Phi = \Phi_0 \sin(\omega_n t + ns + \eta)$ and $r = r_0 \cos(\omega_n t + ns + \eta)$, for $n \neq 0$, if the determinant of the system of equations is zero,

$$\left(c_\gamma \omega_n + \frac{2c_\kappa n(1 - n^2)}{R_0^3} \right)^2 - c_\kappa \left(-\frac{2c_\gamma n \omega_n}{R_0} + c_\kappa \frac{(1 - n^2)^2}{R_0^4} \right) \left(1 + \frac{n^2 - 1/2}{R_0^2} \right) = 0. \tag{5.19}$$

which provides the following dispersion relations

$$\frac{c_\gamma}{c_\kappa} \omega_n \approx -\frac{n + |n|}{R_0} \mp \frac{1 - n^2 \pm n|n| + n^4}{2|n| R_0^3} + \mathcal{O}\left(\frac{1}{R_0} \right). \tag{5.20}$$

As expected from the chiral properties of the skyrmion, the frequency takes different values for positive and negative n, corresponding to counterclockwise and clockwise motion respectively. In

these specific cases, we can write

$$\omega_n \approx \begin{cases} \frac{2nc_\kappa}{c_\gamma R_0}, & \text{for } n < 0, \\[2mm] \frac{c_\kappa(1+n^4)}{2c_\gamma|n|R_0^3}, & \text{for } n > 0, \end{cases} \tag{5.21}$$

which corresponds to the higher order excitation modes reported by *Kravchuk et al.* [75] For the modes with $n = 0$, we consider only the dynamics due to a dimensionless scaling factor of the radius and a global rotation for Φ. If the oscillations in Φ are small, one obtains the frequency dependence as

$$\omega \approx \frac{\tilde{c}_\kappa}{c_\gamma R_0^2}. \tag{5.22}$$

This breathing mode is also in agreement with the assymptotics found from the spin wave spectrum calculation. [75]
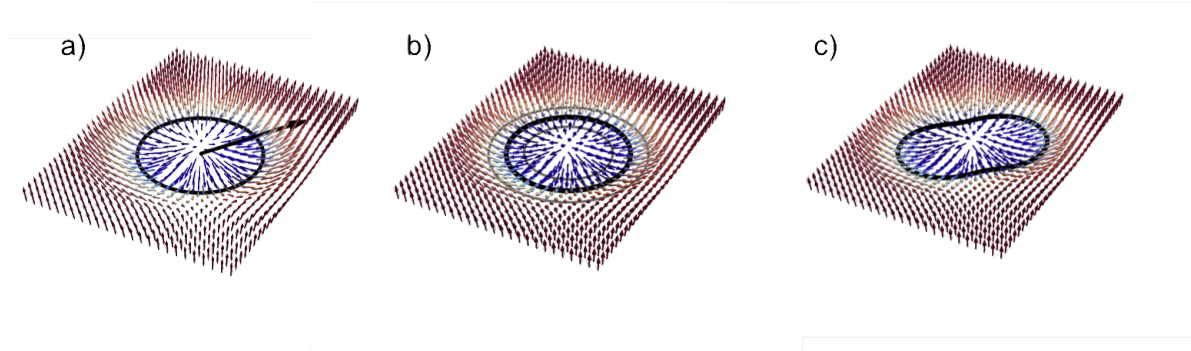
Figure 5.4: A sketch of the skyrmion modes. (a) represents the translational mode $n = \pm 1$, it corresponds to the rigid motion of the skyrmion. It is a zero-mode of the system if the Hamiltonian is invariant under translations. [4] (b) represents the breathing mode $n = 0$, it correspond to a scaling dynamics of the skyrmion. In systems with no chiral interactions, this mode is also a zero mode. [5] (c) represents the mode $n = 2$, it corresponds to a change in the shape of the skyrmion. The modes with $|n| > 1$ assume poligonal shapes. Their dynamics correspond to a rigid rotation around the center of the skyrmion.

The modes in equations 5.21 and 5.22 correspond to the excitation modes of the skyrmion, see Figs. 5.4 and 5.5 . [4, 5, 73, 74, 75] The $n = 0$ and $n = \pm 1$ modes do not change the

overall shape of the skyrmion, they are the breathing and translational modes. For higher $|n|$, one obtain the excitation modes that change the shape of skyrmions, taking polygonal forms. These modes are associated to bounded magnon modes. It has been shown that they can be associated to an effective mass for skyrmions. [74, 4] The higher order modes have not been individually observed yet experimentally and usually require sophisticated numerical methods to be obtained analytically. The formalism presented in this chapter allows for a natural way to obtain these modes non-radially symmetric modes. Moreover, it can be extended for the study of excitation modes of worm domains and other structures observed in experiments.

Figure 5.5: Image concerning the higher order excitation modes of skyrmion. In this figure, we present a sketch of the polygonal shapes of the higher order excitations. Reprinted from Ref. [3] with permission.

6. CONCLUSIONS

In this Thesis we analyzed the current and magnetic field driven dynamics of topological magnetic textures from an effective point of view. By stability, scaling and symmetries arguments, we were able to: i) propose means to inject domain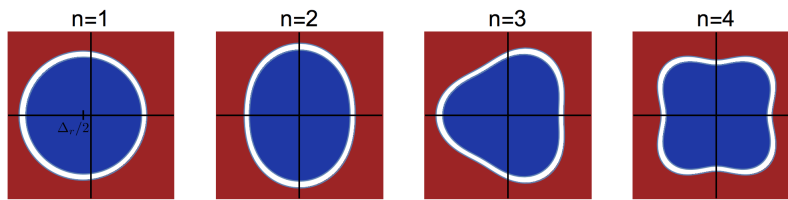 walls into ferromagnetic nanowires by all electrical means with a minimal micromagnetic model; ii) propose a model independent Hamiltonian formalism to describe the current and magnetic field driven domain wall dynamics in both FM and AFM materials; iii) obtain an effective theory for domain walls in ferromagnetic thin films that included the bending of domain walls. This latest formalism allowed us to unify the treatment of large skyrmions and domain wall strings. The main feature of the presented work was to analyze the dynamics of a highly complex non-linear, non-local equation with infinite degrees of freedom by considering just a set of dynamical parameters. This process is independent of micromagnetic details and fluctuations, due to a difference in the scales of the observed phenomena. The effective description proved to be a powerful and rich method, which allows for an intuitive understanding of the general dynamics. Well known aspects of the topological magnetic dynamics can be reproduced in a natural way from the effective descriptions. Moreover, since it is possible to easily introduce new interactions and consider new conditions, it permits the study of novel mechanisms. The ideas and formalisms presented in this Thesis are crucial for the proposal of a new generation of memory devices based on magnetic features.

The main work on this Thesis was based in three papers published on Physical Review B. [1, 2, 3] The published results have been written in Chapters 3,4 and 5. In the first paper, Chapter 3, we studied the DW injection by electrical means in a specific configuration for a ferromagnetic nanowire with a strong pinning center. We have shown that there is a maximum current, called critical current v_s^c, for which the magnetic configuration is static and stable. For currents above the critical current there is a periodic injection of DWs into the nanowire. The period is given by a universal exponent and, in general, is independent of microscopic details. This physics is described in terms of the time evolution of a single parameter that defines the static configurations below

the critical current. It is derived from a minimal Hamiltonian that does not contain "twisting" terms or applied magnetic field. The introduction of twisting terms, however, can reduce the critical current. In the second paper, Chapter 4, we have developed a Hamiltonian approach to the current and magnetic field driven dynamics of both ferromagnetic and antiferromagnetic DWs. We assume that DWs are rigid topological objects. The dynamics are obtained from a universal set of equations in terms of phenomenological constants and pairs of dynamical parameters. The formalism is capable to solve various problems of both FM and AFM DW dynamics on the same footing and includes extensions to different geometries and new interactions. The Hamiltonian formalism developed is rich and powerful. It reproduces well known dynamics and allows for a natural way to study new phenomena. By considering the combination of perpendicular magnetic field, anisotropy and electrical current, we obtained an orientation switch mechanism for AFM DWs that can be experimentally measured in the future and be useful for memory devices. In the third paper, Chapter 5, we extended the description of domain walls as one dimensional objects to include new degrees of freedom along the DW. The string description of the DW is a powerful method that allows for the analysis of several experimentally observed behaviors, including curved DWs and spin wave propagation along DWs. Moreover, it unifies the description of elongated domain walls and skyrmions in the large radius limit. We obtained an effective action for the DW string in terms of a pair of soft mode fields, from which one obtains the full undamped dynamics. We applied the formalism to describe the excitation modes of skyrmions. We considered only periodic boundary conditions for the DW string. For more general dynamics of string DWs, it is required to include boundary terms. They can be treated by adding effective potentials.

To conclude, the theory presented in this thesis is mostly independent of micromagnetic details. It can be applied to a vast range of conditions and not only reproduces the well known physics reported in the literature as it allows for the study of new observable behaviors. The formalisms can be easily extended to consider new interactions and geometries. This is an essential step for developing a new generation of memory devices based on topological magnetic textures.

REFERENCES

[1] M. Sitte, K. Everschor-Sitte, T. Valet, D. R. Rodrigues, J. Sinova, and A. Abanov, "Current-driven periodic domain wall creation in ferromagnetic nanowires," *Physical Review B*, vol. 94, p. 064422, aug 2016.

[2] D. R. Rodrigues, K. Everschor-Sitte, O. A. Tretiakov, J. Sinova, and A. Abanov, "Spin texture motion in antiferromagnetic and ferromagnetic nanowires," *Physical Review B*, vol. 95, p. 174408, may 2017.

[3] D. R. Rodrigues, A. Abanov, and J. Sinova, "Effective description of domain wall strings," pp. 1–9, 2017.

[4] C. Schütte and M. Garst, "Magnon-skyrmion scattering in chiral magnets," *Physical Review B*, vol. 90, p. 094423, sep 2014.

[5] D. D. Sheka, B. A. Ivanov, and F. G. Mertens, "Internal modes and magnon scattering on topological solitons in two-dimensional easy-axis ferromagnets," *Physical Review B*, vol. 64, p. 024432, jun 2001.

[6] S. Bader and S. Parkin, "Spintronics," *Annual Review of Condensed Matter Physics*, vol. 1, pp. 71–88, aug 2010.

[7] H. N. Khan, D. A. Hounshell, and E. R. H. Fuchs, "Science and research policy at the end of Moore's law," *Nature Electronics*, vol. 1, no. 1, pp. 14–21, 2018.

[8] G. E. Moore, "Cramming more components onto integrated circuits, Reprinted from Electronics, volume 38, number 8, April 19, 1965, pp.114 ff.," *IEEE Solid-State Circuits Society Newsletter*, vol. 11, pp. 33–35, sep 2006.

[9] M. M. Waldrop, "More than Moore," *Nature*, vol. 530, pp. 144–147, feb 2016.

[10] V. Zhirnov, R. Cavin III, J. Hutchby, and G. I. Bourianoff, "Limits to binary logic switch scaling - a gedanken model," vol. 91, pp. 1934 – 1939, 12 2003.

[11] D. Weller and A. Moser, "Thermal effect limits in ultrahigh-density magnetic recording," *IEEE Transactions on Magnetics*, vol. 35, pp. 4423–4439, Nov 1999.

[12] S. D. Bader, "Colloquium: Opportunities in nanomagnetism.," *Reviews of Modern Physics*, 2006.

[13] S. S. P. Parkin, M. Hayashi, and L. Thomas, "Magnetic Domain-Wall Racetrack Memory," *Science*, vol. 320, pp. 190–194, apr 2008.

[14] S. A. Wolf, A. Y. Chtchelkanova, and D. M. Treger, "Spintronics?A retrospective and perspective," *IBM Journal of Research and Development*, vol. 50, pp. 101–110, jan 2006.

[15] N. Nagaosa and Y. Tokura, "Topological properties and dynamics of magnetic skyrmions.," *Nature Nanotechnology*, vol. 8, pp. 899–911, dec 2013.

[16] N. Romming, C. Hanneken, M. Menzel, J. E. Bickel, B. Wolter, K. von Bergmann, A. Kubetzka, and R. Wiesendanger, "Writing and Deleting Single Magnetic Skyrmions," *Science*, vol. 341, pp. 636–639, aug 2013.

[17] A. Fert, N. Reyren, and V. Cros, "Magnetic skyrmions: advances in physics and potential applications," *Nature Reviews Materials*, vol. 2, no. 7, p. 17031, 2017.

[18] S. Woo, K. Litzius, B. Krüger, M.-y. Im, L. Caretta, K. Richter, M. Mann, A. Krone, R. M. Reeve, M. Weigand, P. Agrawal, I. Lemesh, M.-A. Mawass, P. Fischer, M. Kläui, and G. S. D. Beach, "Observation of room-temperature magnetic skyrmions and their current-driven dynamics in ultrathin metallic ferromagnets," *Nature Materials*, vol. 15, pp. 501–506, feb 2016.

[19] W. Jiang, P. Upadhyaya, W. Zhang, G. Yu, M. B. Jungfleisch, F. Y. Fradin, J. E. Pearson, Y. Tserkovnyak, K. L. Wang, O. Heinonen, S. G. E. te Velthuis, and A. Hoffmann, "Blowing magnetic skyrmion bubbles," *Science*, vol. 349, no. 6245, pp. 283–286, 2015.

[20] F. Matsukura, Y. Tokura, and H. Ohno, "Control of magnetism by electric fields," *Nature Nanotechnology*, vol. 10, no. 3, pp. 209–220, 2015.

[21] J. Sampaio, V. Cros, S. Rohart, A. Thiaville, and A. Fert, "Nucleation, stability and current-induced motion of isolated magnetic skyrmions in nanostructures," *Nature Nanotechnology*, vol. 8, pp. 839–844, oct 2013.

[22] S. Emori, U. Bauer, S.-M. Ahn, E. Martinez, and G. S. D. Beach, "Current-driven dynamics of chiral ferromagnetic domain walls.," *Nature Materials*, vol. 12, pp. 611–6, jul 2013.

[23] A. Thiaville, S. Rohart, É. Jué, V. Cros, and A. Fert, "Dynamics of Dzyaloshinskii domain walls in ultrathin magnetic films," *EPL (Europhysics Letters)*, vol. 100, p. 57002, dec 2012.

[24] A. Hubert and R. Schäfer, *Magnetic Domains*. Berlin, Heidelberg: Springer Berlin Heidelberg, 3rd ed., 1998.

[25] L. D. Landau and E. M. Lifshitz, "On the Theory of the Dispersion of Magnetic Permeability in Ferromagnetic Bodies," *Phys. Zeitsch. der Sow.*, vol. 8, pp. 153–169, 1935.

[26] T. Skyrme, "A non-linear field theory," *Proceedings of the Royal Society A: Mathematical, Physical and Engineering Sciences*, vol. 260, aug 1961.

[27] M. Yamanouchi, D. Chiba, F. Matsukura, and H. Ohno, "Current-induced domain-wall switching in a ferromagnetic semiconductor structure," *Nature*, vol. 428, pp. 539–542, apr 2004.

[28] G. Tatara and H. Kohno, "Theory of Current-Driven Domain Wall Motion: Spin Transfer versus Momentum Transfer," *Physical Review Letters*, vol. 92, p. 086601, feb 2004.

[29] M. Hayashi, L. Thomas, C. Rettner, R. Moriya, X. Jiang, and S. S. P. Parkin, "Dependence of current and field driven depinning of domain walls on their structure and chirality in permalloy nanowires," *Physical Review Letters*, vol. 97, no. 20, pp. 1–4, 2006.

[30] A. Bogdanov and D. Yablonskii, "Thermodynamically stable "vortices" in magnetically ordered crystals. The mixed state of magnets," *Zh. Eksp. Teor. Fiz.*, vol. 95, no. 1, p. 178, 1989.

[31] A. Bogdanov and A. Hubert, "Thermodynamically stable magnetic vortex states in magnetic crystals," *Journal of Magnetism and Magnetic Materials*, vol. 138, pp. 255–269, dec 1994.

[32] S. Muhlbauer, B. Binz, F. Jonietz, C. Pfleiderer, A. Rosch, A. Neubauer, R. Georgii, and P. Boni, "Skyrmion Lattice in a Chiral Magnet," *Science*, vol. 323, pp. 915–919, feb 2009.

[33] N. L. Schryer and L. R. Walker, "The motion of 180° domain walls in uniform dc magnetic fields," *Journal of Applied Physics*, vol. 45, no. 12, p. 5406, 1974.

[34] N. Papanicolaou and T. N. Tomaras, "Dynamics of magnetic vortices," *Nuclear Physics, Section B*, vol. 360, pp. 425–462, aug 1991.

[35] O. Tretiakov, D. Clarke, G.-W. Chern, Y. B. Bazaliy, and O. Tchernyshyov, "Dynamics of Domain Walls in Magnetic Nanostrips," *Physical Review Letters*, vol. 100, p. 127204, mar 2008.

[36] S. Komineas and N. Papanicolaou, "Skyrmion dynamics in chiral ferromagnets," *Physical Review B*, vol. 92, p. 064412, 2015.

[37] T. Gilbert, "Classics in Magnetics A Phenomenological Theory of Damping in Ferromagnetic Materials," *IEEE Transactions on Magnetics*, vol. 40, pp. 3443–3449, nov 2004.

[38] D. E. Eastman, F. J. Himpsel, and J. A. Knapp, "Experimental band structure and temperature-dependent magnetic exchange splitting of nickel using angle-resolved photoemission," *Phys. Rev. Lett.*, vol. 40, pp. 1514–1517, Jun 1978.

[39] I. E. Dzyaloshinskii, "Thermodynamic theory of weak ferromagnetism in antiferromagnetic substances," *Sov. Phys. JETP*, vol. 5, p. 1259, 1957.

[40] T. Moriya, "New Mechanism of Anisotropic Superexchange Interaction," *Physical Review Letters*, vol. 4, pp. 228–230, mar 1960.

[41] M. Bode, M. Heide, K. von Bergmann, P. Ferriani, S. Heinze, G. Bihlmayer, A. Kubetzka, O. Pietzsch, S. Blügel, and R. Wiesendanger, "Chiral magnetic order at surfaces driven by inversion asymmetry," *Nature*, vol. 447, pp. 190–193, may 2007.

[42] M. Hoffmann, B. Zimmermann, G. P. Müller, D. Schürhoff, N. S. Kiselev, C. Melcher, and S. Blügel, "Antiskyrmions stabilized at interfaces by anisotropic Dzyaloshinskii-Moriya interaction," *Nature Communications*, vol. 8, p. 308, feb 2017.

[43] H. J. G. Draaisma and W. J. M. De Jonge, "Surface and volume anisotropy from dipole-dipole interactions in ultrathin ferromagnetic films," *Journal of Applied Physics*, vol. 64, no. 7, pp. 3610–3613, 1988.

[44] P. M. Chaikin and T. C. Lubensky, *Principles of condensed matter physics*, vol. 67. 1995.

[45] O. Tchernyshyov, "Conserved momenta of a ferromagnetic soliton," *Annals of Physics*, vol. 363, pp. 98–113, 2015.

[46] D. Ralph and M. D. Stiles, "Spin transfer torques," *Journal of Magnetism and Magnetic Materials*, vol. 320, pp. 1190–1216, apr 2008.

[47] A. Thiaville, Y. Nakatani, J. Miltat, and Y. Suzuki, "Micromagnetic understanding of current-driven domain wall motion in patterned nanowires," *Europhysics Letters (EPL)*, vol. 69, pp. 990–996, mar 2004.

[48] J. C. Slonczewski, "Currents and torques in metallic magnetic multilayers," *Journal of Magnetism and Magnetic Materials*, vol. 247, no. 3, pp. 324–338, 2002.

[49] Z. Li and S. Zhang, "Domain-Wall Dynamics and Spin-Wave Excitations with Spin-Transfer Torques," *Physical Review Letters*, vol. 92, p. 207203, may 2004.

[50] S. Zhang, P. Levy, and A. Fert, "Mechanisms of Spin-Polarized Current-Driven Magnetization Switching," *Physical Review Letters*, vol. 88, p. 236601, may 2002.

[51] N. Papanicolaou, "Antiferromagnetic domain walls," *Physical Review B*, vol. 51, no. 21, pp. 15062–15073, 1995.

[52] T. Jungwirth, X. Marti, P. Wadley, and J. Wunderlich, "Antiferromagnetic spintronics," *Nature Nanotechnology*, vol. 11, no. 3, pp. 231–241, 2016.

[53] A. B. Shick, S. Khmelevskyi, O. N. Mryasov, J. Wunderlich, and T. Jungwirth, "Spin-orbit coupling induced anisotropy effects in bimetallic antiferromagnets: A route towards antiferromagnetic spintronics," *Physical Review B*, vol. 81, p. 212409, jun 2010.

[54] Z. Wei, A. Sharma, A. Nunez, P. M. Haney, R. A. Duine, J. Bass, A. H. MacDonald, and M. Tsoi, "Changing Exchange Bias in Spin Valves with an Electric Current," *Physical Review Letters*, vol. 98, p. 116603, mar 2007.

[55] S. R. Park, C. H. Kim, J. Yu, J. H. Han, and C. Kim, "Orbital-Angular-Momentum Based Origin of Rashba-Type Surface Band Splitting," *Physical Review Letters*, vol. 107, p. 156803, oct 2011.

[56] J. Wu, D. Carlton, J. S. Park, Y. Meng, E. Arenholz, A. Doran, A. T. Young, A. Scholl, C. Hwang, H. W. Zhao, J. Bokor, and Z. Q. Qiu, "Direct observation of imprinted antiferromagnetic vortex states in CoO/Fe/Ag(001) discs," *Nature Physics*, vol. 7, pp. 303–306, apr 2011.

[57] X. Marti, I. Fina, C. Frontera, J. Liu, P. Wadley, Q. He, R. J. Paull, J. D. Clarkson, J. Kudrnovský, I. Turek, J. Kuneš, D. Yi, J.-H. Chu, C. T. Nelson, L. You, E. Arenholz, S. Salahuddin, J. Fontcuberta, T. Jungwirth, and R. Ramesh, "Room-temperature antiferromagnetic memory resistor.," *Nature Materials*, vol. 13, pp. 367–374, apr 2014.

[58] E. V. Gomonay and V. M. Loktev, "Spintronics of antiferromagnetic systems (Review Article)," *Low Temperature Physics*, vol. 40, pp. 17–35, jan 2014.

[59] S. Rohart and A. Thiaville, "Skyrmion confinement in ultrathin film nanostructures in the presence of Dzyaloshinskii-Moriya interaction," *Physical Review B*, vol. 88, p. 184422, nov 2013.

[60] P. Milde, D. Köhler, J. Seidel, L. M. Eng, A. Bauer, A. Chacon, J. Kindervater, S. Mühlbauer, C. Pfleiderer, S. Buhrandt, C. Schütte, and A. Rosch, "Unwinding of a skyrmion lattice by magnetic monopoles.," *Science*, vol. 340, pp. 1076–1080, may 2013.

[61] A. Bogdanov, "New localized solutions of the nonlinear field equations," *JETP Letters*, vol. 62, no. 3, pp. 231–235, 1995.

[62] V. Pokrovsky, "Properties of ordered, continuously degenerate systems," *Advances in Physics*, vol. 28, pp. 595–656, oct 1979.

[63] A. Bobeck, P. Bonyhard, and J. Geusic, "Magnetic bubbles?An emerging new memory technology," *Proceedings of the IEEE*, vol. 63, no. 8, pp. 1176–1195, 1975.

[64] M. Ezawa, "Giant skyrmions stabilized by dipole-dipole interactions in thin ferromagnetic films," *Phys. Rev. Lett.*, vol. 105, p. 197202, Nov 2010.

[65] A. Vansteenkiste, J. Leliaert, M. Dvornik, M. Helsen, F. Garcia-Sanchez, and B. Van Waeyenberge, "The design and verification of MuMax3," *AIP Advances*, vol. 4, no. 10, pp. 0–22, 2014.

[66] "MicroMagnum — Fast Micromagnetic Simulator for Computations on CPU and GPU." available online at micromagnum.informatik.uni-hamburg.de.

[67] D.-S. Han, S.-K. Kim, J.-Y. Lee, S. J. Hermsdoerfer, H. Schultheiss, B. Leven, and B. Hillebrands, "Magnetic domain-wall motion by propagating spin waves," *Applied Physics Letters*, vol. 94, no. 11, p. 112502, 2009.

[68] M. Garst, J. Waizner, and D. Grundler, "Collective spin excitations of helices and magnetic skyrmions: review and perspectives of magnonics in non-centrosymmetric magnets," *Journal of Physics D: Applied Physics*, vol. 50, p. 293002, jul 2017.

[69] C. Herring and C. Kittel, "On the theory of spin waves in ferromagnetic media," *Phys. Rev.*, vol. 81, pp. 869–880, Mar 1951.

[70] A. V. Chumak, V. I. Vasyuchka, A. A. Serga, and B. Hillebrands, "Magnon spintronics," *Nature Physics*, vol. 11, pp. 453–461, jun 2015.

[71] A. A. Thiele, "Sready-state motion of magnetic domains," *Physical Review Letters*, vol. 30, no. 6, p. 230, 1973.

[72] A. Kosevich, B. Ivanov, and A. Kovalev, "Magnetic Solitons," *Physics Reports*, vol. 194, pp. 117–238, oct 1990.

[73] S.-Z. Lin, C. D. Batista, and A. Saxena, "Internal modes of a skyrmion in the ferromagnetic state of chiral magnets," *Physical Review B*, vol. 89, p. 024415, jan 2014.

[74] I. Makhfudz, B. Krüger, and O. Tchernyshyov, "Inertia and Chiral Edge Modes of a Skyrmion Magnetic Bubble," *Physical Review Letters*, vol. 109, p. 217201, nov 2012.

[75] V. P. Kravchuk, D. D. Sheka, U. K. Rößler, J. van den Brink, and Y. Gaididei, "Spin eigenmodes of magnetic skyrmions and the problem of the effective skyrmion mass," *Physical Review B*, vol. 97, p. 064403, feb 2018.

[76] J. Slonczewski, "Excitation of spin waves by an electric current," *Journal of Magnetism and Magnetic Materials*, vol. 195, no. 2, pp. L261–L268, 1999.

[77] K. Everschor, M. Garst, R. A. Duine, and A. Rosch, "Current-induced rotational torques in the skyrmion lattice phase of chiral magnets," *Physical Review B*, vol. 84, p. 064401, aug 2011.

[78] D. Clarke, O. Tretiakov, G.-W. Chern, Y. B. Bazaliy, and O. Tchernyshyov, "Dynamics of a vortex domain wall in a magnetic nanostrip: Application of the collective-coordinate approach," *Physical Review B*, vol. 78, p. 134412, oct 2008.

[79] R. Tomasello, E. Martinez, R. Zivieri, L. Torres, M. Carpentieri, and G. Finocchio, "A strategy for the design of skyrmion racetrack memories," *Scientific Reports*, vol. 4, p. 6784, may 2015.

[80] O. A. Tretiakov, Y. Liu, and A. Abanov, "Domain-Wall Dynamics in Translationally Nonivariant Nanowires: Theory and Applications," *Physical Review Letters*, vol. 108, p. 247201, jun 2012.

[81] M. Hayashi, L. Thomas, R. Moriya, C. Rettner, and S. S. P. Parkin, "Current-Controlled Magnetic Domain-Wall Nanowire Shift Register," *Science*, vol. 320, pp. 209–211, apr 2008.

[82] A. Yamaguchi, T. Ono, S. Nasu, K. Miyake, K. Mibu, and T. Shinjo, "Real-space observation of current-driven domain wall motion in submicron magnetic wires," *Phys. Rev. Lett.*, vol. 92, p. 077205, Feb 2004.

[83] D. A. Allwood, "Magnetic Domain-Wall Logic," *Science*, vol. 309, no. 5741, pp. 1688–1692, 2005.

[84] K. Everschor-Sitte, M. Sitte, T. Valet, A. Abanov, and J. Sinova, "Skyrmion production on demand by homogeneous DC currents," *New Journal of Physics*, vol. 19, p. 092001, sep 2017.

[85] J. C. Slonczewski, C. D. Graham, and J. J. Rhyne, "DYNAMICS OF MAGNETIC DOMAIN WALLS," vol. 170, pp. 170–174, 1972.

[86] O. A. Tretiakov and A. Abanov, "Current Driven Magnetization Dynamics in Ferromagnetic Nanowires with a Dzyaloshinskii-Moriya Interaction," *Physical Review Letters*, vol. 105, p. 157201, 2010.

[87] A. Brataas, Y. Tserkovnyak, and G. E. W. Bauer, "Magnetization dissipation in ferromagnets from scattering theory," *Physical Review B*, vol. 84, p. 054416, aug 2011.

[88] R. A. Duine, "Spintronics: An alternating alternative.," *Nature Materials*, vol. 10, no. 5, pp. 344–345, 2011.

[89] E. G. Tveten, A. Qaiumzadeh, O. Tretiakov, and A. Brataas, "Staggered Dynamics in Antiferromagnets by Collective Coordinates," *Physical Review Letters*, vol. 110, p. 127208, mar 2013.

[90] R. Cheng and Q. Niu, "Dynamics of antiferromagnets driven by spin current," *Physical Review B*, vol. 89, p. 081105, feb 2014.

[91] J. Kim, J. Sinha, S. Mitani, M. Hayashi, S. Takahashi, S. Maekawa, M. Yamanouchi, and H. Ohno, "Anomalous temperature dependence of current-induced torques in CoFeB/MgO heterostructures with Ta-based underlayers," *Physical Review B*, vol. 89, p. 174424, 2014.

[92] R. Cheng, M. W. Daniels, J.-G. Zhu, and D. Xiao, "Ultrafast switching of antiferromagnets via spin-transfer torque," *Physical Review B*, vol. 91, no. 6, p. 064423, 2015.

[93] Y. Kim, S. Member, X. Fong, K.-w. Kwon, M.-c. Chen, and K. Roy, "Multilevel Spin-Orbit Torque MRAMs," *IEEE Transactions on Magnetics*, vol. 62, no. 2, pp. 561–568, 2015.

[94] E. G. Tveten, A. Brataas, and Y. Tserkovnyak, "Electron-magnon scattering in magnetic heterostructures far out of equilibrium," *Physical Review B*, vol. 92, p. 180412, nov 2015.

[95] T. Jungwirth, V. Novák, X. Martí, M. Cukr, F. MácA, A. B. Shick, J. Mašek, P. Horodyská, P. Němec, V. Holý, J. Zemek, P. Kužel, I. Němec, B. L. Gallagher, R. P. Campion, C. T. Foxon, and J. Wunderlich, "Demonstration of molecular beam epitaxy and a semiconducting band structure for I-Mn-V compounds," *Physical Review B*, vol. 83, p. 035321, 2011.

[96] X. Martí, B. G. Park, J. Wunderlich, H. Reichlová, Y. Kurosaki, M. Yamada, H. Yamamoto, A. Nishide, J. Hayakawa, H. Takahashi, and T. Jungwirth, "Electrical measurement of antiferromagnetic moments in exchange-coupled IrMn/NiFe stacks," *Physical Review Letters*, vol. 108, no. January, pp. 017201(1)–017201(4), 2012.

[97] H. Gomonay and V. Loktev, "Hydrodynamic theory of coupled current and magnetization dynamics in spin-textured antiferromagnets," *arXiv*, may 2013.

[98] H. V. Gomonay and V. M. Loktev, "Spin transfer and current-induced switching in antiferromagnets," *Physical Review B*, vol. 81, p. 144427, apr 2010.

[99] P. Wadley, B. Howells, J. Elezny, C. Andrews, V. Hills, R. P. Campion, V. Novak, K. Olejnik, F. Maccherozzi, S. S. Dhesi, S. Y. Martin, T. Wagner, J. Wunderlich, F. Freimuth, Y. Mokrousov, J. Kune, J. S. Chauhan, M. J. Grzybowski, A. W. Rushforth, K. W. Edmonds, B. L. Gallagher, and T. Jungwirth, "Electrical switching of an antiferromagnet," *Science*, vol. 351, pp. 587–590, feb 2016.

[100] J. Shibata, G. Tatara, and H. Kohno, "Effect of Spin Current on Uniform Ferromagnetism: Domain Nucleation," *Physical Review Letters*, vol. 94, p. 076601, feb 2005.

[101] L. Liu, T. Moriyama, D. C. Ralph, and R. A. Buhrman, "Spin-Torque Ferromagnetic Resonance Induced by the Spin Hall Effect," *Physical Review Letters*, vol. 106, p. 036601, jan 2011.

[102] S. W. Jiang, S. Liu, P. Wang, Z. Z. Luan, X. D. Tao, H. F. Ding, and D. Wu, "Exchange-Dominated Pure Spin Current Transport in Alq3 Molecules," *Physical Review Letters*, vol. 115, p. 086601, aug 2015.

[103] S. Emori, E. Martinez, K.-J. Lee, H.-W. Lee, U. Bauer, S.-M. Ahn, P. Agrawal, D. C. Bono, and G. S. D. Beach, "Spin Hall torque magnetometry of Dzyaloshinskii domain walls," *Physical Review B*, vol. 90, p. 184427, nov 2014.

[104] M. J. Benitez, A. Hrabec, A. P. Mihai, T. A. Moore, G. Burnell, D. McGrouther, C. H. Marrows, and S. McVitie, "Magnetic microscopy and topological stability of homochiral Néel domain walls in a Pt/Co/AlOx trilayer," *Nature Communications*, vol. 6, p. 8957, 2015.

[105] O. Boulle, J. Vogel, H. Yang, S. Pizzini, D. de Souza Chaves, A. Locatelli, T. O. Mente?, A. Sala, L. D. Buda-Prejbeanu, O. Klein, M. Belmeguenai, Y. Roussigné, A. Stashkevich, S. M. Chérif, L. Aballe, M. Foerster, M. Chshiev, S. Auffret, I. M. Miron, and G. Gaudin, "Room-temperature chiral magnetic skyrmions in ultrathin magnetic nanostructures," *Nature Nanotechnology*, vol. 11, pp. 449–454, jan 2016.

[106] a. E. LaBonte, "Two-dimensional Bloch-type domain walls in ferromagnetic films," *Journal of Applied Physics*, vol. 40, no. 6, pp. 2450–2458, 1969.

[107] I. E. Dzyaloshinskii, "A thermodynamic theory of ?weak? ferromagnetism of antiferromagnetics," *Journal of Physics and Chemistry of Solids*, vol. 4, pp. 241–255, jan 1958.

[108] L. Chen, F. Matsukura, and H. Ohno, "Direct-current voltages in (Ga,Mn)As structures induced by ferromagnetic resonance.," *Nature Communications*, vol. 4, p. 2055, jan 2013.

[109] O. Boulle, S. Rohart, L. D. Buda-Prejbeanu, É. Jué, I. M. Miron, S. Pizzini, J. Vogel, G. Gaudin, and A. Thiaville, "Domain Wall Tilting in the Presence of the Dzyaloshinskii-

Moriya Interaction in Out-of-Plane Magnetized Magnetic Nanotracks," *Physical Review Letters*, vol. 111, p. 217203, nov 2013.

[110] C. B. Muratov, V. V. Slastikov, A. G. Kolesnikov, and O. A. Tretiakov, "Theory of the dzyaloshinskii domain-wall tilt in ferromagnetic nanostrips," *Phys. Rev. B*, vol. 96, p. 134417, Oct 2017.

[111] J. Müller, "Magnetic skyrmions on a two-lane racetrack," *New Journal of Physics*, vol. 19, p. 025002, feb 2017.

[112] C. Du, H. Wang, F. Yang, and P. C. Hammel, "Enhancement of Pure Spin Currents in Spin Pumping Y 3 Fe 5 O 12 / Cu / metal Trilayers through Spin Conductance Matching," *Journal of Applied Physics*, vol. 117, no. May, p. 172603, 2015.